ORBIT CONTROL FOR A SPACECRAFT AROUND A SPLITTING CONTACT BINARY ASTEROID

BY
JEAN-BAPTISTE BOUVIER

THESIS

Submitted in partial fulfillment of the requirements
for the degree of Master of Science in Aerospace Engineering
in the Graduate College of the
University of Illinois at Urbana-Champaign, 2018

Urbana, Illinois

Adviser :

Assistant Professor Koki Ho

ABSTRACT

This thesis examines an orbit control problem for a spacecraft around a contact binary asteroid considering the dynamics of both the spacecraft and the asteroid itself. It is known that approximately 15% of the near-Earth asteroids are binary, and among these the fraction of contact binaries is between 6 and 10% [1]. Most contact binary asteroids are constituted of an agglomeration of smaller boulders maintained together due to their internal gravity, which is a relatively unstable configuration. Therefore, even a minor change in their mass distribution, like would be caused by the landing of mining machines, can result in a modification of the asteroid's structure including a landslide or a splitting. Particularly, separation of the asteroid into two parts is problematic in terms of orbit control, because of the consequences on the gravitational field of the asteroid. Traditional two-body orbital control methods cannot be applied to the missions to those asteroids because they do not consider the dynamic activities of the asteroids themselves. This thesis proposes and evaluates a control method to follow a predefined path under unknown states of the splitting binary asteroid.

ACKNOWLEDGEMENTS

I would like to thank my advisor, Professor Koki Ho* for being an exceptional mentor. From our first meeting he introduced me to really interesting research topics, and always helped me going through every difficulty.

This work would not have been possible without the expertise on asteroids of Professor Masatoshi Hirabayashi† who introduced us to this promising topic. A more extended version of the work done in this thesis will be published in a journal paper [2].

I am indebted to my Engineering School ISAE-Supaéro, for enabling this dual degree program and giving me the opportunity and all the assistance to apply and be accepted in a prestigious Graduate program.

I am also grateful to the University of Illinois for the funding opportunities through the Teaching Assistantship and Grader positions.

*Assistant Professor, Aerospace Engineering, 306 Talbot Laboratory, MC-236, 104 South Wright Street, Urbana, Illinois 61801
†Assistant Professor, Aerospace Engineering, Auburn University, 211 Davis Hall, Auburn, AL 36849

Contents

1. Introduction

Recent emphasis on space explorations of asteroids has arisen in the last decades. Such explorations include collecting asteroid materials for multiple purposes that widely range from scientific studies to engineering advances. Hayabusa, an asteroid sample return mission led by Japan Aerospace Exploration Agency (JAXA), explored Itokawa, an asteroid orbiting close to the Earth, or a so-called Near-Earth Asteroid (NEA), and brought a sample of its surface material back to the Earth [3]. As of November 2018, JAXA-led Hayabusa2 [4] and NASA-led OSIRIS-REx [5, 6] are currently attempting to sample such material from target asteroids (162183) Ryugu and (101955) Bennu, respectively, with different technologies. The Hayabusa2 mission plans to land on Ryugu's surface, ignite a high-speed projectile to surface rocks, and collect fragmented materials inside a sampling system, called the sampler horn [4]. On the other hand, the OSIRIS-REx mission attempt to expel a jet of gas to capture surface rocks [6]. In addition, as a NASA/New Frontiers-level mission, CAESAR, one of two selected NASA/New Frontiers-level missions, is proposed to explore and return a sample of 67P/Churyumov-Gerasimenko, a comet whose orbit is mostly controlled by Jupiter, i.e. a Jupiter Family Comet [7].

These asteroid exploration missions have shown potential expansion of our capabilities for proximity operations to the surface of asteroids. Complex operations in concepts and ongoing missions include direct interactions of spacecrafts with surface materials [8] or the structure of asteroids due to explosion [9]. Also, collecting a large amount of materials from asteroid surfaces, or so-called asteroid mining [10], or deflecting potential hazardous asteroids by using kinetic impactors are part of applications and utilization of asteroids that require sophisticated technologies. NASA Double Asteroid Redirect Test (DART) is an ongoing mission, which is in Phase C, as of November 2018 [11]. In this mission, the DART spacecraft is designed to impact on a smaller secondary component of (65803) Didymos, a binary NEA but is also planned to release a Cube-Sat before the impact.

Such advanced proximity operations may change the gravitational configuration of a target asteroid. There are two reasons to address this issue. First, many small asteroids may be gravitational aggregates of small boulders, rocks, and regoliths, or so-called rubble piles as inferred from the spin conditions of observed asteroids [12] and from the derived bulk density and surface morphology of Itokawa [3] . Such asteroids do not have mechanical strengths [13, 14], implying that they might occasionally experience local and global landslides and internal deformation processes. These processes have been proposed to result from fast rotation and tidal effects. The second reason is that asteroids are irregularly shaped. Typically, their various shapes are categorized into four critical shapes: spheroidal, elongated,

contact binary, and non-classified shapes. Importantly, the shape is a critical parameter of the rotationally induced deformation mode [15].

Earlier work showed that when the shape of an asteroid changes, the gravity field of that asteroid also changes, leading to additional perturbation of the orbital motion. [16] demonstrated how the mutual motion of Didymos could change due to the shape deformation of the primary body. The latter may significantly control the magnitude of the centrifugal force, depending on the bulk density of this asteroid. They considered that at this fast rotation condition, if the primary body receives a kinetic energy input (from an impact), the current shape configuration would become unstable and settle into a new one. They identified that such a process significantly changes the gravity field, causing orbital perturbation.

We cast the following questions. How does the orbital motion of a spacecraft change when the asteroid is structurally deformed during proximity operations? And, how robustly should control and navigation systems work to guide the spacecraft securely? This scenario may be likely to happen as proximity operations to asteroids become more complex. As mentioned above, some asteroids have fast rotation rate, which cause higher sensitivity to structural deformation as centrifugal forces become dominant. In this case, shape deformation may occur due to small inputs that trigger large deformation. Also, when a spacecraft conducts impact operations, the crater formation processes cause critical deformation processes including compression beneath the surface and the formation of circular depression.

In this works, we consider an hypothetical situation in which our spacecraft is performing proximity operations near a contact binary asteroid – an asteroid that consists of two lobes connecting with each other – that gradually deforms. Ground observations have shown that a contact binary configuration is common in the Solar System, in fact 15% of observed asteroids may have some features of contact binaries [1, 17] . For instance 1996 HW1 [18], Itokawa [3], (Figure 1) Castalia [19], and Toutatis [20] in near earth asteroids (NEAs) and Kleopatra [21] in the main belt asteroids (MBAs) are contact binary asteroids. For cometary nuclei, observations have revealed that about 70% of the observed objects at high resolution may be contact binaries. The nucleus of 67P/Churyumov-Gerasimenko is one of comets having a contact binary nucleus. A potential formation scenario of this object include a catastrophic disruption followed by a soft contact of two lobes and recontact after splitting of two lobes. If a contact binary asteroid reaches its critical limit of a structural condition, the neck part experiences inelastic deformation, causing the body to stretches along the minimum moment of inertia axis gradually [14]. To consider this condition, we introduce a simple model in which a contact binary is assumed to be a system that has two spherical bodies connecting with each other.

We demonstrate a control and navigation technique for robustly achieving a desired trajectory. We made some assumptions to implement our orbital control technique. First, the spacecraft possesses sensors to measure its relative distance and velocity with respect to a considered contact binary asteroid. We propose a navigation technique where the spacecraft estimates the asteroids' mass ratio, and total inertia during operation, given measurement noise. To implement this method, we apply an Extended Kalman Filter (EKF)[22, 23]. A path following algorithm developed by

[24] is used to keep the spacecraft on the desired orbit. Thus, our main system includes a plant, a controller, and an estimator. This organization is based on Adaptive Control [25–27].

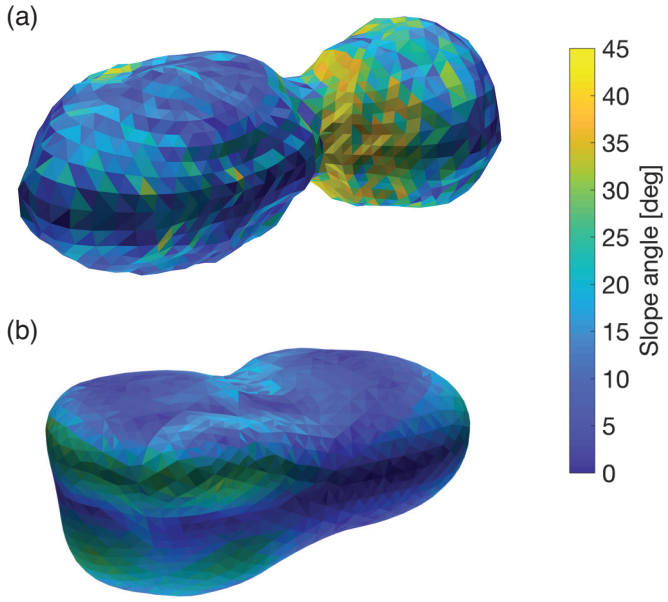

Fig. 1 Examples of contact binary asteroids. a. 1996 HW1 [18], and b. Castalia [19]. The contour shows the slope angle, which is an angle between the force direction (gravitational plus centrifugal forces) and an inward vector normal to the surface.

2. Literature Review

Our work is at the crossover of several different domains among which are orbital mechanics, adaptive control and asteroid modeling. An extensive literature covers all these topics but no paper (to the best of our knowledge) tackles them all at once. This is the objective of our thesis: to bring these topics together through the study of a trajectory control problem around a splitting asteroid.

2.1. Asteroids

2.1.1. Asteroid model

Several asteroid models have been developed in the literature, ranging from the simplest one that considers just a point-mass, to a very complex model with polyhedral representation. Werner and Scheeres [28] compares three types of high fidelity gravitation models: the Harmonic expansion of the gravity potential field, the Mascon model, and the Polyhedron representation. The Harmonic series have a guaranteed convergence. Their precision can be controlled easily by truncation and the literature available on this topic is abundant. Yet, this method has three main drawbacks: it is never exact, always an approximation of the actual field; the series can diverge inside the circumscribing sphere of the asteroid, which is a problem for the close surface gravity of non-spherical bodies; and the model does not provide a way to know the spatial position of the surface of the asteroid, so another algorithm must be implemented to know if a point is inside or outside the asteroid. Mascon is the abbreviation of mass concentration. This term is used because the method models the body as a collection of point masses whose locations and masses are chosen to match the total mass of the asteroid and approximate the overall gravitation field. Like the Harmonic procedure, it does not carry information about the surface position, and is usually less accurate for the same calculation time. In the Mascon model, the gravity field does not diverge, but the convergence to the actual gravitation field with the increase of the distance to the asteroid is slower than for Harmonics. A polyhedron is a solid 3D body which is constituted of planar faces meeting at straight edges or points. It can be non-convex, with interior voids, holes, etc. It is assumed to have a constant density. This model is proven better than the two previous ones, since the error is reduced to a shape determination process, the gravity field does not diverge and it brings along an easy way to acquire the spatial position of the surface. However the computations are more time expensive. Our work does not yet require such a precision, and thus a much simpler model has been adopted.

The asteroids' model considered in this thesis is composed of two spheres rotating around each other and linked with a massless rod. Since the spheres are homogeneous and the spacecraft does not perform any close surface operation, the point-mass model can be adopted for each asteroid. This model has also been employed by M. Hirabayashi [15], which studies the stability of the Lagrange points (explanations in section 3.3) in the case of a contact binary asteroid

submitted to a centripetal force stronger than the gravitational one. The two interesting Lagrange points L_2 and L_3 for orbit purposes remain unstable, and thus we should still be able to compute the usual Halo orbits around those points. We will tackle this topic later, in section 3.3.

2.1.2. Orbital Mechanics applied to Asteroids

Orbiting around a small body like an asteroid is a challenging task due to the sharp variations of gravity caused by its irregular shape. [29] highlighted this sensitivity by computing several orbits with close initial conditions, but very different endings: impact, escape or stability. The solar attraction and radiation pressure are also two sources of instability that must be accounted for. The study is then divided into two regimes: Gravity Regime, when the asteroid provides the main perturbation; and the Solar Dominated Regime. In that first scenario, depending if the asteroid rotates uniformly or tumbles, equilibrium points and periodic orbits are respectively dense or discrete. An accurate model of the asteroid and of its gravitation potential is required for the computations of these close orbits. In the second scenario, a criteria is derived to check if the spacecraft will escape its periodic orbit due to the action of the Sun. And eventually the study of the spacecraft Rosetta orbiting the comet 67P/Churyumov-Gerasimenko, gather this two scenarios into one real test case. The closer the orbit is to the comet, the more unstable it is, because of the variation of the gravitation field, but for further away orbits, the action of the Sun becomes the main source of destabilization. They finally determined Terminator orbits that remain indefinitely stable, and are thus a good choice for the mission.

To study a binary asteroid, the 2 Body Problem (2BP) frame is a good first step. Yet the point mass assumption is not valid anymore when considering non-spherical bodies, close operations, or the rotation of the asteroids. Therefore the 2BP has been extended by taking into account the mass distribution of the primaries to become the Full 2 Body Problem (F2BP). A simplified version of the F2BP is studied by Bellerose and Scheeres [30] by restricting the bodies shape to a spheroid and an ellipsoid. This work goes further in term of stability study than Scheeres [31], and also investigates the various periodic orbits of one body around the other along with their stability. Depending on the mass ratio $\nu = \frac{m_{sphere}}{m_{sphere}+m_{ellipse}}$, there is one or two equilibrium positions. When the ellipsoid dominates there is one equilibrium, and when increasing the mass ratio, i.e. going towards a sphere dominated system, it bifurcates into two equilibrium : one stable, and one unstable. Orbits around those equilibrium points can be computed using eigenvectors perturbation and Poincarré maps. More details about orbit calculations can be found in section 4.1.2.

Once this F2BP is totally explored, one can move further, and tackle the motion of a spacecraft in the surroundings of two asteroids. Its trajectory can then be calculated in the frame of the Restricted Full 3 Body Problem (RF3BP). It is called Restricted because this case has the primary assumption that the third body (the spacecraft) has a negligible mass compared to the asteroids'. Therefore, the first two bodies are not affected by the spacecraft's position and follow the F2BP. In Bellerose and Scheeres [32] a periodic motion of the primaries is chosen as solution of the F2BP, and several orbits of the spacecraft in that environment are studied. Their stability is heavily impacted by the choice of the F2BP

motion.

2.1.3. Asteroid Missions

The objective of this thesis is to provide some useful knowledge for an asteroid mission design dealing with risks of splitting. Several asteroid missions have already been successfully launched by different space agencies. We will review the OSIRIS-REx and Hayabusa missions, respectively led by NASA and JAXA.

The main goal of the Origins, Spectral Interpretation, Resource Identification, and Security–Regolith Explorer (OSIRIS-REx) asteroid mission is to return a sample from the asteroid (101955) Bennu. This mission will improve our knowledge about asteroids, and more specifically about the chemical, thermal, and mineralogical properties of the regolith. Lauretta et al. [5] study the properties of Bennu, while Lauretta et al. [6] proposes a mission overview with detailed lists of objectives and system engineering processes. Asteroids are composed of leftover materials from the Solar System formation that didn't aggregate to form a planet, and thus stayed intact since that time. Indeed, the rocks composing a planet have been considerably altered because of numerous impacts, they melted with each other to form new rocks, and the atmosphere can also totally modify them. Having access to such old materials can help understand the initial conditions on Earth that led to the apparition of life. The visited asteroid is of a completely different kind compared to the target of the previous asteroid missions, in terms of shape and albedo. The orbit of Bennu is known with one of the best accuracy and approach the Earth every 6 years. A high fidelity trajectory model has been established by taking into account all planets and even more than a dozen of other asteroids able to perturb the orbit of Bennu. The YORP effect has also been accounted for in the model. All the information concerning Bennu are the result of a long astronomical campaign of observations. A study of the surroundings of Bennu has also been led, in order to assess the presence of undetected small asteroids or dust orbiting Bennu. With the detailed knowledge acquired, the authors were able to produce a time-line of the events resulting in the asteroid as we can observe it now. But they were also capable to predict its trajectory for the next two centuries, until the point were the probability of impact with the Earth becomes too high. The mission is divided into several phases : launch, outbound cruise, approach, rendezvous trajectory, orbit around the asteroid for several months in order to totally map its surface and select candidate sampling sites. Then, once one has finally been approved, the touch-and-go operations will be rehearsed several times before performing all five of them to recover samples. The mission will enable a close study of the YORP effect and bring more details about how to account for it. Indeed, it is the main mechanism that drives small asteroids out of their orbit in the main asteroid belt, until possibly intersecting Earth's orbit. From a mission design point of view, several parameters of the asteroid were crucial in the target selection process, namely the orbit, mass, shape, rotation, gravity, temperature,... Indeed, only NEA were considered due to delta-V capabilities of the sample return spacecraft. And even among those, the propellant cost of the round-trip trajectory brought selective constraints. Then small asteroids have been rejected because rotating too fast. If all the feasibility and safety criteria are verified, then the scientific value of the remaining candidates is the final

selection judge. The spacecraft overview can help giving realistic values to our simulations. Touch-and-Go Sample Acquisition Mechanism, or TAGSAM will collect materials by releasing a jet of N_2 gas on the surface and then capture the floating particles blown from the surface. The flight control of the spacecraft is crucial for that kind of maneuver and must be of high precision. However, working in a micro-gravity environment dangerously increases the impact of every little uncertainty in the thrust control. The OSIRIS-REx mission will test all the asteroids rendezvous procedures, the specific sampling method, validate the asteroid's model built from ground observations. Overall it should benefit all the future NEA approach missions by bringing more knowledge about their formation and concerning the YORP effect.

The Japan Aerospace Exploration Agency has already successfully accomplished an asteroid sample return mission named Hayabusa on the S-type asteroid Itokawa, and is currently implementing Hayabusa2 on another near-Earth asteroid but of a more rare carbonaceous-type (C-type) called Ryugu.

Fujiwara et al. [3] describe the asteroid Itokawa with the data collected by Hayabusa. Similarly to the OSIRIS-REx mission, the target asteroid has been selected because easily reachable due to a small inclination and an orbit crossing the Earth orbit. After some time spent into orbit for mapping and topographic purposes a touch-down site has been selected in the Muses Sea. The sampling method is the main difference with the OSIRIS-REx mission. In this case, the spacecraft lands and stays half an hour on the asteroid surface, before going back on orbit. When on the ground, surface materials were supposed to be captured by the horn system. Yet it failed, only floating dust has been collected. But these few particles were still a high valued asset, and enabled sufficient analysis to consider the mission as a success. Several mechanical failures prevented to reach the desired precision in the mass determination of Itokawa and delayed the samples return. Several hypothesis try to explain the presence of small particles of regolith on the surface of Itokawa even if they should be at their escape velocity. Based on the slope and the distribution of the boulder sizes at the surface several tentative explanations of the past and the internal structure of the asteroid.

Tsuchiyama et al. [33] analyze the regolith samples returned by Hayabusa. The particles have been compared with the Moon samples, and also with meteorite rocks. They deduced that chondrites, the most common meteorite rocks found on Earth come from S-type asteroids like Itokawa, which are also the most common NEO. From the shape and size distribution of the samples, a tentative history of Itokawa has been selected. A parent asteroid has been impacted, blowing away rocks from its surface. Those had close trajectories because of a common ejection, and have collided and agglomerated forming the rubble-pilesItokawa as we know it.

Watanabe et al. [4] provide a mission overview of Hayabusa2. The target asteroid, Ryugu is of the C-type, which is the category expected to date back from the beginning of the Solar System, and composed of a mixture of minerals, ice, and organic matter. The spacecraft is carrying three small rovers and a lander. The latter can hop on the asteroid's surface to visit several zones of the asteroid. Indeed, the spacecraft will only perform touch-and-go maneuvers, and so will not stay long enough on the surface to perform close science analysis. The sampling method is different than the two previous ones. When the spacecraft will reach the surface, a small projectile will be expelled at a speed of $300m/s$

to pulverize the surface of Ryugu, and the floating particles will be captured by the sampling horn. This operation will be repeated at three different locations on the asteroid. To get access to underground materials, an artificial crater will be formed by a copper impactor. It will be detached from the spacecraft, and collide only when the craft is safely positioned on the other side of Ryugu. The crater is expected to have a diameter of up to 10 meters. When the dust and projectiles created by the impact will be cleared out, the spacecraft can perform its last sampling maneuver in the crater. The scientific goal of the mission is to understand the origin of water and organic matter on the Earth, by studying the distribution and the characteristics of the materials composing Ryugu.

The sampling processes implemented during the three asteroid missions presented, will most likely be light enough not to jeopardize the asteroid's unstable structure. Therefore, the case of the splitting of the asteroids has never been mentioned or studied, but can become crucial when studying smaller asteroids or heavier surface operations like mining.

2.1.4. Characteristics of Binary Asteroids

Before considering the splitting of a binary asteroid, it is wise to learn about its formation. The contact binaries usually result from the collision of two bodies orbiting each other. [34] describes how a single asteroid can become such a non-contact binary system. In that work, an asteroid is modeled by a collection of small spheres in contact, because most asteroids are rubble piles. Then the YORP (Yarkovsky–O'Keefe–Radzievskii–Paddack) effect is applied to the model : it consists in a slow spin-up of an asteroid due to the photons flux from the Sun. When its rotating velocity becomes sufficiently high, the spheres composing the model move from the poles to the equator where they have a faster velocity, and can thus be ejected. Depending on the shape of the asteroid, and on the coefficients of the collision model between two spheres, the ejecta staying on orbit can gather and form a second body orbiting the initial asteroid. By this process a single asteroid becomes a pair of two rotating asteroids. By the continuous increase of rotating velocity and the perturbing tidal forces due to encounters with planets, these two asteroids can collapse back together and form a contact binary asteroid.

Several mechanisms perturb the angular momentum of asteroids. These include the YORP effect, but also direct impacts and the tidal effect due to planetary flybys. On average they tend to increase the rotating velocity. These mechanisms are all capable of splitting a single asteroid into two bodies as we have seen previously, and also of dividing a contact binary asteroid. This last scenario has been studied by Scheeres [31], and more specifically the case of a spheroidal asteroid interacting with an ellipsoid one. Both of these bodies tend to evolve towards their overall minimum-energy configuration, which can either be one asteroid resting on the other along one of its principal axes of inertia, or the two bodies rotating around each other at a specific angular velocity.

The fission limit is the minimal rotating velocity required to lose contact between the primaries and transit from a resting equilibrium to an orbital one. The mass distribution of the asteroids and their shape have a considerable impact on their fission limit. The typical value of this limit corresponds to a period of 2.2 hours, which is faster than almost all

binary asteroids in the Near Earth Objects (NEO) population. However, when considering an ellipsoid and spheroid system, instead of a double spheroids system, the fission limit can be considerably lowered. Indeed, if the ellipsoid is bigger than the spheroid, then the fission limit period can increase to around 6 hours. This case is more common among the NEO, which means that a larger number of asteroids could be at their fission limit. Thus the splitting of binary asteroids is more probable than expected for the slow rotating NEO, and learning how to deal with this case motivates this thesis. Several scenarios of lifetime evolution of asteroids are studied by Scheeres [31] based on the mass ratio. If the ellipsoid is largely dominant, then the fission is likely to happen and the system can also have a positive free-energy, meaning that the bodies can escape each others' attraction. For an ellipsoid a bit less dominant (like Itokawa [3]) the free-energy would be negative, and since the orbital equilibrium positions are mostly unstable, the asteroids could re-impact. But the most common case pictures a dominant spheroidal primary, or two spheroidal bodies which have stable equilibrium and a faster fission limit.

2.2. Adaptive Control

2.2.1. Theory of Adaptive Control

The environment of the spacecraft is constantly evolving and only accessible through imperfect measurements. To model these uncertainties and account for unknown parameters (such as the asteroids masses, inertia,...), an adaptive control organization is necessary [26]. Adaptive control is usually divided into two broad categories : direct and indirect control. The latter category is the more natural process since it estimates the unknown parameters of the system, before using them in the control law. Direct methods combine these two steps by calculating directly the control gains; the plant parameters are not estimated. Even if these two approaches are philosophically different, they can be equivalent in some cases [35]. A good introduction to the adaptive control theory would be Lavretsky [25], because the amateur has first to go through all the Lyapunov stability theory. Indeed, to prove the stability of a controller the most widely used method is to define an appropriate candidate Lyapunov function $V(x)$, positive definite, with continuous partial derivatives and whose time derivative along any state trajectory $x(t)$ is negative semi-definite. After proving all the necessary theorems, one can use this method and actually build an adaptive controller along one of the two usual scheme : the Model Reference Adaptive Controller (MRAC) and the Self Tuning Controller (STC). They can both be direct or indirect.

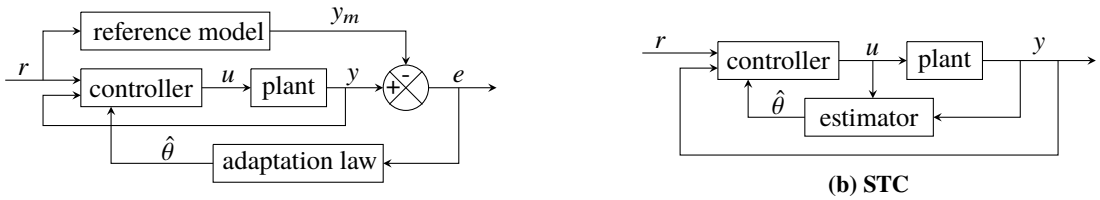

(a) MRAC **(b) STC**

Fig. 2 The two different adaptive controllers

The overall goal of those controllers is to have the output $y(t)$ following a reference input $r(t)$. Some adaptive control law can achieve it, even with several estimated parameters not converging to their true value. Thus, having the estimation error going to zero can be seen as a secondary goal, but its accomplishment will facilitate reaching the overall goal. So let us work on the Indirect method, since it estimates the parameters of the system to compute the best control law. Estimator and controller are two different blocks, as can be seen in fig. 2b, therefore the controller assumes that its inputs are the true parameters, and not their estimates. This is the Certainty Equivalence Principle (CEP). To ensure the convergence of the estimated parameters to their true values, a condition on the input signal ν is required: the Persistency of Excitation (PE). ν is PE if and only if $\exists\ \alpha > 0\ /\ \forall t > 0, \exists\ T > 0\ /\ \int_t^{t+T} \nu(\tau)\nu(\tau)^T d\tau > \alpha I_N$. The math linking convergence and PE are developed in Boyd and Sastry [36] and rely on Harmonic Analysis. Their conclusion is that the spectrum of the reference input r must contain at least N frequencies in order to ensure the convergence of N estimated parameters.

Therefore a control strategy relying on the CEP needs a control signal persistently excited. However, in practice the PE conditions are difficult to meet. Thus, more contemporary papers have focused on relaxing these PE conditions. The idea behind the PE conditions is that the input must be rich enough, carry sufficient information to allow the estimator to work properly. One can draw a parallel with the need of N independent equations in order to determine N unknowns. A PE signal carries at all time enough information. But, if the system can store data, then after some time, a signal less rich can also have brought a sufficient amount of information. This is the idea more formally developed by Chowdhary and Johnson [37].

2.2.2. Spacecraft Adaptive Control

The literature tackling Adaptive Control for spacecrafts mainly focuses at estimating and controlling the craft's attitude, i.e. its orientation with respect to an inertial reference frame. Usually the moments of inertia of the spacecraft are known with some uncertainties, and the adaptive control law derived from a feedback linearization of the equations of motion (EOM), will try to overcome those uncertainties to successfully complete the mission.

J. Junkins and Robinett [38] consider a spacecraft with unknown inertia trying to perform a maneuver. After establishing the EOM and making use of the adapted attitude representation, an adaptive feedback controller is calculated. The process follows the classical steps :

- Taking the difference between the actual and reference EOM, to obtain the perturbation equation
- Inverting this equation to access the control input u
- Choosing u while building V a candidate Lyapunov function in order to prove the stability of the controller
- Computing the estimates of a few gains

This paper employs a Direct Adaptive Control method by estimating directly control gains. Since the PE conditions are not assumed to be verified, the estimates are not assured to converged to their true value, but the controller is still

working because not relying on the CEP.

In that same framework, S. Bandyopadhyay and Hadaegh [39] consider a space object retrieval's mission. The spacecraft's inertia is considered known, but a large captured object is rigidly attached to the vehicle, so the overall inertia is unknown. A feedback linearization control law is implemented. The authors highlight the crucial result that due to the uncertainties on the moments of inertia, certain terms usually considered as negligible perturbations in the control law are in fact big enough to reach the maximum control capability of the vehicle. Therefore a specifically designed feedback control plus Proportional Integral Derivative (PID) control law has been implemented and proven to converge exponentially. Several variations of this controller have been compared, and a simple but efficient D+PD version picturing a switch from Derivative to Proportional Derivative control when the object's spin has been cancelled. Every control law described in this paper make use of the Derivative control, which requires knowledge about the time derivative of the desired trajectory.

P. Singla and Junkins [40] apply adaptive control methods to a position and attitude spacecraft control. Since the objective is to perform an autonomous docking, a high level of precision and robustness are required. The EOM are calculated in the Local-Vertical-Local-Horizontal (LVLH) frame. Position and velocity errors are used to build the Lyapunov function, while considering that position is acquired with measurements noise. The convergence is obviously impacted by the noise level, and only when set to zero, in an ideal case, can the global asymptotic stability be guaranteed. The process to tackle position and attitude control is exactly the same, only the EOM differs. The results are validated through numerical simulations for a poorly known spacecraft's mass and inertia.

Almost all the the adaptive attitude control algorithms rely on the CEP as remarked by Seo and Akella [41]. Yet this assumption made by the controller is almost always wrong because the estimated parameters are not equal to their true values and that results in a degradation of the performances. Indeed, the PE conditions are not practical to implement, because the richness required in the signal usually consists in extra components that are not needed otherwise, and thus results in an excessive amount of input used. Several restrictive assumptions are made in this paper, mainly that the only unknowns are constant and a full state feedback is available. By using the Immersion and Invariance adaptive control theory [27] and an attractive manifold, the authors manage to build a controller not relying on the CEP. Its convergence is once again proven with the Lyapunov stability theory. Yet the main drawback of this method is that the parameter estimation error z does not necessarily converge to zero. Indeed for a signal W_f, only $\lim_{t\to\infty} W_f(t)z(t) = 0$ is guaranteed. To sum up, the controller works without a PE signal but does not ensure the estimates convergence. It can therefore be applied in a Direct Adaptive framework, where the parameters convergence is not one of the objectives since the estimates are gains and not physical parameters of the model.

All these papers assume that a desired motion and its time derivatives are available. They are required for several crucial steps : designing the controller and then proving its stability.

3. Asteroid Modeling

3.1. Modeling of dynamics about a contact binary asteroid

As we have seen in section 2.1.1 several modeling methods are available for an asteroid. A spherical harmonics model [28] may work at some level but may not be suitable for calculation of the gravity field inside the circumferential radius of the contact binary body, or known as the XXX sphere. To this date, the most feasible model may be a polyhedron shape model that consists of a pile of tiles to generate the topography of an asteroid shape. Many trajectory analyses about an irregularly shaped have been performed to better understand the complex orbital feature about such an object. Yet it requires heavy calculations, and thus is not a good choice for a first simple model, but can be considered to improve our method in a future work.

In this work, we apply a simple asteroid model that mimics the gravity field of a contact binary asteroid [15]. This asteroid model consists of two spherical lobes that are connected with each other by a massless bar fig. 7. It initially rotates along the maximum moment of inertia axis with a spin rate Ω_0. The masses of a larger lobe and a smaller lobe are m_1 and m_2, with radii being respectively r_1 and r_2. The radii are linked the parameter α

$$r_1 = \alpha\, r_2 \qquad with\ \alpha \geqslant 1 \tag{1}$$

The distance between the centers of mass of these lobes is defined as d. Each lobe has the same bulk density ρ. We will work with the coordinate frame rotating with this asteroid. Its axes are: x along the minimum moment of inertia axis, z along the axis of rotation, and y in the orthogonal direction.

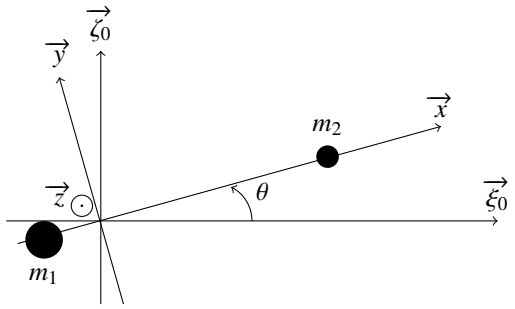

Fig. 3 Inertial and Rotating frames

Earlier work brought the following equation. Does an asteroid keep the original shape all the time? If not, how can a spacecraft dynamically behave? This question comes from the fact that many small asteroids are rubble piles, objects that are made by accumulations of small rocks and regoliths (the term of regolith was originally used by Sheomaker to describe small fragments on the Moon). The main asteroid belt is a violent environment in space, because

asteroids undergo high-velocity impacts, tidal effects, fast rotations, YORP effect, etc. All these processes cause shape deformations of the asteroids. In the present work, we consider a shape deformation process due to the fast rotation of a contact binary asteroid.

This asteroid is targeted for a sampling or mining mission involving an orbiter and a lander. After several months of orbits around the body, a precise surface map has been established and a landing site has been selected. Yet the internal structure of the asteroid is still largely unknown because assessed only through the gravitational perturbations affecting the orbit of the spacecraft. We assume that the asteroid is a rubble piles and is thus highly unstable. The landing of the machines, or their excavation activity then produce an impact important enough to destabilize the asteroid, and it splits at its weakest point: the junction between the two lobes. Since the rotating velocity of the asteroid was high enough, the two parts then start to split. The objective of our mission is to keep the spacecraft on its orbit encircling both primaries. There is obviously a time limit at this goal if the primaries completely diverge from each other. We will then try to make the orbiter follow its elliptical path for one revolution.

3.2. Two Body Problem Study

In this work, after the lander causes the splitting of the asteroids, the spacecraft has no more direct impact on the asteroids' motion. Indeed, its mass is negligible with respect to that of the asteroids. Thus their motion can be derived by solving the Two Body Problem (2BP) equations. All the equations are written using the coordinates of the frame rotating with the asteroids. They both remain on the X-axis, and their motion can be characterized by the following parameters : d their splitting distance, Ω the angular velocity of the rotating frame, and m_1 and m_2 the masses of the two asteroids. Ω is defined as the time derivative of θ, the angle between the inertial reference frame and the rotating one. The equation of motion of the asteroids in the rotating frame can be written as :

$$\ddot{d} = d\Omega^2 - G\frac{(m_1 + m_2)}{d^2} \qquad with \quad G = 6.67408 \times 10^{-20}\ km^3 kg^{-1} s^{-2} \tag{2}$$

This equation gives the position of each asteroid. Indeed, by using the normalized constant mass parameter $\mu = \frac{m_2}{m_1+m_2}$ with $m_2 \leq m_1$, it is possible to ascertain the positions of each primary along the X-axis : $-\mu d$ for m_1 and $(1-\mu)d$ for m_2.

Yet the angular velocity is also a function of the distance d. We first need the moment of inertia I of the asteroid. Considering two homogeneous spheres of radii r_1 and r_2, of masses m_1 and m_2 and separated with a distance d, the total inertia is:

$$I(d) = \frac{2}{5}\left(m_1 r_1^2 + m_2 r_2^2\right) + \frac{m_1 m_2}{m_1 + m_2} d^2 = I_{spheres} + m_1 \mu d^2 \tag{3}$$

Let us introduce $m_{tot} = m_1 + m_2$ the total mass of the asteroids, and the normalized inertia of the spheres: $I_n = \frac{I_{spheres}}{m_{tot}}$

. Remarking that $m_1 = (1-\mu)m_{tot}$, we obtain:

$$\frac{I(d)}{m_{tot}} = I_n + \mu(1-\mu)d^2 \tag{4}$$

We normalize the inertia to have a variable of the same amplitude as the other components of the state vector. And now using the conservation of the angular momentum L, the angular velocity $\Omega(d)$ is linked to the splitting distance d :

$$L = I(d)\,\Omega(d) = I(d_0)\,\Omega(d_0) = I(d_0)\,\Omega_0 \tag{5}$$

Ω_0 being the initial rotating velocity of the asteroid. Then by normalizing this previous equation the angular velocity is reduced to $\Omega(d) = \Omega_0 \frac{I(d_0)}{m_{tot}} \frac{m_{tot}}{I(d)} = \Omega_0 \left(\frac{I_n + \mu(1-\mu)d_0^2}{I_n + \mu(1-\mu)d^2} \right)$. Which can now be introduced in eq. (2) to give a differential equation with only one variable d :

$$\ddot{d} = d\Omega_0^2 \left(\frac{I_n + \mu(1-\mu)d_0^2}{I_n + \mu(1-\mu)d^2} \right)^2 - \frac{Gm_{tot}}{d^2} \tag{6}$$

As can be seen in the equation obtained from Newton's Second Law eq. (2), two opposite forces are applied on d : the gravitation that tends to bring the bodies closer and the centrifugal acceleration which has a repulsive action. Due to this opposition, an equilibrium exists and can be found by plugging $\ddot{d} = 0$ in eq. (2), and gives $\Omega_{eq}(R) = \sqrt{\frac{G(m_1+m_2)}{R^3}}$ with R the distance between the centers. When considering the initial situation with the contact binary asteroids, their initial angular velocity Ω_0 is arbitrary. The model adopted for the splitting operation assumes that the angular velocity is conserved. Then Ω_0 can be compared to $\Omega_{eq}(d_0)$ to predict the future motion of the asteroids.

- if $\Omega_{eq}(d_0) > \Omega_0$ the gravitation force is stronger than the centrifugal one, and thus the asteroids will not split, but stay in contact.
- if $\Omega_{eq}(d_0) < \Omega_0$ then the asteroids have enough energy to overcome the potential energy barrier and their splitting distance d will grow to infinity.

Only the second scenario is considered in this paper. This case brings restrictions on the period of the orbit of the spacecraft since once the smaller asteroid is out of the ellipse, the gravitational perturbations are too large for the craft to remain on the desired orbit.

3.3. Lagrange Points

To observe the asteroids several kinds of orbits can do the job. When considering the situation before splitting, so only one asteroid, the natural orbit choice would be circular or elliptical. This choice of orbit is considered in this paper. And even after the splitting, the control law aims at having the spacecraft remain on that two-bodies orbit.

Another approach would be to consider the situation after the splitting as reference for the orbit choice. Indeed, in

the context of the 3BP other types of orbits become available. They are located around the gravitational equilibrium points of the system, which are called the Lagrange points and denoted L_i with $i \in \{1, 2, 3, 4, 5\}$.

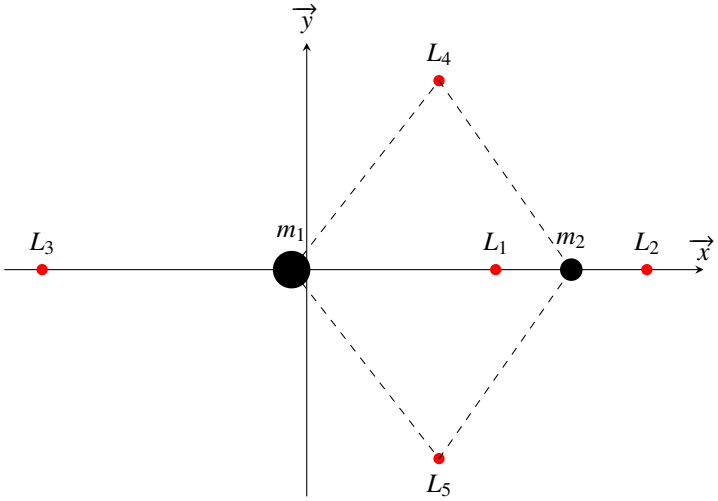

Fig. 4 Equilibrium points of the circular restricted 3 Body Problem

For $i \in \{1, 2, 3\}$, L_i is dynamically unstable, thus orbits exist around these three collinear Lagrange points. Several different families of orbit exist among which are the HALO, Distant Retrograde Orbits (DRO), Planar Lyapunov orbits, Vertical Lyapunov,... However a necessary condition for these orbits to exist is that the Lagrange point considered is far enough from the asteroid. In fact in our case of a contact binary system, L_1 is initially inside the asteroid. Therefore an orbit around L_1 is impossible before the splitting. For L_2 and L_3 the answer is not as easy. Depending on the asteroids' mass ratio they can be inside or outside of the asteroids.

Computing the position of the three collinear Lagrange points boils down to solving a quintic polynomial function, as described in the book John E Prussing [42].

$$(M_1 + M_2)X^5 + (3M_1 + 2M_2)X^4 + (3M_1 + M_2)X^3 - (3M_3 + M_2)X^2 - (2M_2 + 2M_3)X - (M_2 + M_3) = 0 \qquad (7)$$

M_1, M_2 and M_3 are masses assigned depending on the case considered. Since they are all positive, the six coefficients written in parenthesis in the previous equation are all positive. Thus the sign of each monomial is written. We can observe that there is only one change of sign, and the polynomials theory tells us that therefore there is only one positive root, which is the solution we are looking for. The solution X can be related to the three positions described in fig. 5 : $X = \frac{x_3 - x_2}{x_2 - x_1}$

For instance if we want to determine the position of L_2, then the three bodies are ordered as m_1, m_2 and spacecraft at L_2, so the mass associated at each positions are : $M_1 = m_1$, $M_2 = m_2$ and $M_3 = 0$. Then we can solve eq. (7) for X. We are interested in $x_3 - x_2$, and we know the distance between primaries $x_2 - x_1$. L_2 being outside of the asteroid means

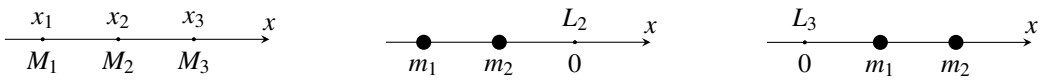

(a) General case **(b) Case : L2** **(c) case : L3**

Fig. 5 Different configurations to determine L_2 or L_3

$x_3 - x_2 > r_2$, i.e. $x_3 - x_2 = X(x_2 - x_1) = X(r_1 + r_2) = X(\alpha r_2 + r_2) = X(1 + \alpha)r_2 > r_2$ so we just want $X(1 + \alpha) > 1$

For L_3 similar calculations lead to $X\frac{\alpha}{1+\alpha} < 1$. fig. 6 shows these two relative distances for $\alpha \in [0, 10]$. In the L_2 case 6a, if $\alpha < 2.847$, then L_2 is outside the asteroid. As for L_3 (6b), it is always outside of the asteroids even if the distance tends towards zero as α increases.

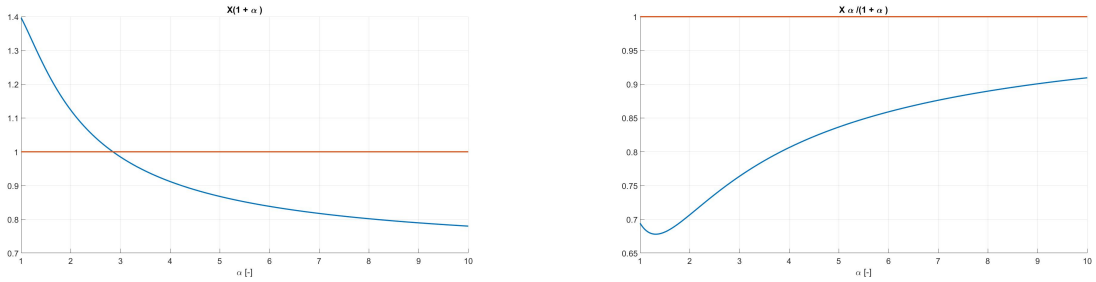

(a) Case : L2 **(b) Case : L3**

Fig. 6 Relative distance between Lagrangian point and the surface of the asteroid as a function of α

Even if fig. 6 shows numerous values of the parameter α allowing the desired Lagrangian point L_i to be outside of the asteroid, this condition is not sufficient. Indeed, there must be enough room around L_i to place an orbit that does not intersect with the surface of the asteroid.

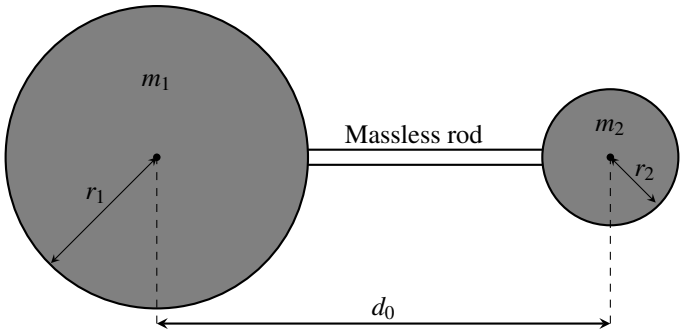

Fig. 7 Asteroid model

Let consider three test cases, the asteroids 1996 HW1 [18], Kleopatra [21] and Castalia [19], [43]. Starting from the actual dimensions of the asteroid, a two-spheres model has been established and its values are gathered in table 1.

They both have a small enough value of α for L_2 to be out of the asteroid. We can now compute the distance of $L_{2,3}$ to the surface of the asteroid. $d_{L_2} = x_3 - x_2 - r_2 = Xd_0 - r_2$, and $d_{L_3} = x_2 - x_1 - r_1 = \frac{d_0}{X} - r_1$. For these

Name	r_1	r_2	α	d_0	ρ	Ω_{eq}	Ω_0
1996 HW1	0.95 km	0.6 km	1.583	2.25 km	2×10^3 kg/m^{-3}	2.2947×10^{-4} rad/s	1.992×10^{-4} rad/s
Kleopatra	49 km	48 km	1.021	179 km	4.85×10^3 kg/m^{-3}	2.323×10^{-4} rad/s	3.2409×10^{-4} rad/s
Castalia	0.46 km	0.4 km	1.15	0.86 km	2.1×10^3 kg/m^{-3}	3.844×10^{-4} rad/s	4.2883×10^{-4} rad/s

Table 1 Values of the parameters of the asteroid model for the test cases

numerical values to have a meaning, we will instead consider the relative distance, with respect to the asteroid radius : $r_{L_2} = \frac{d_{L_2}}{r_2} = \frac{Xd_0}{r_2} - 1$ and $r_{L_3} = \frac{d_{L_3}}{r_1} = \frac{d_0}{Xr_1} - 1$.

Name	X_{L_2}	d_{L_2}	r_{L_2}	X_{L_3}	d_{L_3}	r_{L_3}
1996 HW1	0.4703	0.4582 km	0.7636	1.1152	1.0675 km	1.1237
Kleopatra	0.6887	75.27 km	1.5681	1.3701	81.6 km	1.666
Castalia	0.6285	0.1405 km	0.3512	1.2745	0.2148 km	0.4669

Table 2 Distance of the Lagrange points

All the numerical values of r_{L_2} and r_{L_3} are smaller than 2. Considering an observation orbit around one of these Lagrange points with a radius equal to the asteroid's radius, then the distance between the asteroid and the spacecraft almost double along the orbit. These orbits are too close to the surface, and that is the reason why they are not selected as candidate orbits in this thesis. Indeed, at this close distance to the surface of the asteroids, a more detailed model of their shape and gravity field is required to obtain accurate results [43]. The conclusion that can be drawn from this study of the Lagrange points position, is that an orbit around those is not adapted to our thesis. Therefore, more classic elliptical orbits are selected.

The three asteroids of the test cases have been selected over several criteria. They are both obviously contact binary asteroids. 1996 HW1 and Castalia are Near Earth Asteroids and can thus be considered for exploration and mining purposes. As can be seen in fig. 1 1996 HW1 also has the shape one would expect for an asteroid that splits up, the two lobes are clearly separated. Yet this asteroid is on the low-end of the asteroids size scale, its density is not known with precision, so its internal composition might not be worth the exploration, and also it does not rotate fast enough to split away : $\Omega_0 < \Omega_{eq}$. For all these reasons, two other test cases are needed. Castalia and Kleopatra meet the previously mentioned requirements : in size and high density for Kleopatra, and they both rotate fast enough to split.

4. Spacecraft Control Law

Considering a mission of exploration and landing on an asteroid, a pair lander/orbiter is the most general configuration. The orbiter collects data to learn about the surface and the internal structure of the asteroid and thus prepares for the landing. In the eventuality of the asteroid splitting due to the lander, the orbiter has to adapt to this new situation by staying on orbit as long as possible. Our objective is to develop a station-keeping method using a low-thrust propulsion system. Assuming as a first approach, that only the asteroids and the spacecraft interact, the global calculation frame is the Restricted Three Body Problem. The Sun's gravitational attractions can be added later as perturbing forces. The attitude determination relies on position and velocity measurements of the spacecraft with respect to the asteroids which are then processed through an Extended Kalman Filter to compute the state. As for the thrust determination, a path following algorithm is implemented and tracks the desired elliptical orbit.

4.1. Implementation

4.1.1. Adaptive Control

As we have seen in section 2.2.1 there are two main categories : direct and indirect adaptive control. Two main reasons motivated the choice of an indirect method in this paper. First from a mission point of view, the orbiter has to collect information about the asteroid to prepare for the landing. Hence estimating the unknown plant parameters is already part of the mission, so these estimates can naturally be used to compute the control input. The other reason is that a Direct Control implementation requires a reference model which is not available in the case studied here. Indeed the first step of the Direct process is to take the difference between the state equation and the reference one to obtain the error $e = x - x_{ref}$. Then its time derivative $\dot{e}$ can be calculated, and used to build a candidate Lyapunov function V. Eventually, the stable control sought for will make $\dot{V} \leq 0$.

In the case considered in this paper, a reference model would be a trajectory to track, i.e. a list of positions, velocities and accelerations of the spacecraft around the asteroids. The positions are always available since the mission requirement is to follow a given geometrical path. However, obtaining velocity and acceleration can only be done through the whole orbit computation.

4.1.2. Orbit Computation

A coasting orbit is usually chosen as reference, in order to minimize the propellant consumption since even in that case, there will still be some thrust required for adjustments and station keeping. The method to compute a periodic coasting orbit is described in Koon et al. [44] :

- finding an initial position-velocity vector. The orbit being planar and symmetric with respect to the X-axis, a

simple first guess vector would be : $X_0 = [x_0, 0, 0, 0, \dot{y}_0, 0]^t$. x_0 is directly linked to the radius of the orbit, so the only free parameter to determine is the initial velocity $\dot{y}_0$. An accurate first guess is $\dot{y}_0 = R_{orbit}\Omega_0 + \sqrt{\frac{Gm_{tot}}{R_{orbit}}}$, with R_{orbit} the radius of the desired orbit;

- propagating the trajectory until it hits the X-axis again. For the orbit to be periodic this final state must be of the following shape : $X_f = [x_f, 0, 0, 0, \dot{y}_f, 0]^t$. For a circular orbit $x_f = -x_0$ and $\dot{y}_f = -\dot{y}_0$. But usually $\dot{x}_f \neq 0$;
- updating the initial state X_0 to drive $\dot{x}_f$ to zero. These adjustments are made with a differential correction algorithm.
- propagating for a whole period once X_0 makes $|\dot{x}_f| \leq \epsilon$ with ϵ the desired precision.

The differential correction process is described in Chapter 4.2 of Koon et al. [44]. Assuming we are starting around X_0 and we want to reach X_{goal} under the natural dynamics $\dot{X} = f(X)$. The process explains how to make small modifications of X_0. Let $\phi : (\tau, X_0) \rightarrow X(t)$ be the flow map, associating an initial state X_0 at t_0 to its value $X(\tau)$ after the natural propagation for a time τ. We want to perturb the initial state with δX_0 and see how the final state is modified. Let $\delta X(\tau)$ be the difference between the perturbed state and the original one, at the time τ, i.e.

$$\delta X(\tau) = \phi(\tau\ ; X_0 + \delta X_0) - \phi(\tau\ ; X_0) \tag{8}$$

We can then use a Taylor expansion. The second term is conserved, while the higher order ones are neglected to obtain:

$$\delta X(\tau) \simeq \frac{\partial \phi(\tau; X_0)}{\partial X_0} \delta X_0 = \Phi(\tau, t_0)\delta X_0 \tag{9}$$

Φ being the State Transition Matrix (STM).

Now we can apply this theory to our case. At the first iteration of the process we started from X_0 and reached X_f at the time t_f, while aiming at X_{goal}. Then $\delta X(t_f) = X_{goal} - X_f \simeq \Phi(t_f, t_0)\delta X_0$ with $\delta X_0 = X_{0,desired} - X_0$ being the only unknown and also the quantity we are looking for. Then to get $X_{0,desired}$ we just need to invert the STM. In our case only two components of the state are impacted: $\dot{y}_0$ and $\dot{x}_f$, so inverting the whole STM is a waste of time, we can directly obtain:

$$\delta \dot{y}_0 = -\dot{x}_f \left(\frac{\partial \dot{x}}{\partial \dot{y}}\right)^{-1} = -\dot{x}_f \left(\Phi(t_f, t_0)_{4,5}\right)^{-1} \tag{10}$$

eq. (10) is very efficient for the fine tuning step, to get an extremely precise value. However, when we start with a value of $\dot{y}_0$ too far off, the correction step is too small. To improve the speed of the process, we first implemented a linear correction model. Let $\psi : \dot{y}_0 \rightarrow \dot{x}_f$ represent the time propagation of the state. Our first approach is a linearization of ψ to find a more accurate $\dot{y}_0$. We implemented a six steps process, repeated until the precision becomes good enough:

- $\dot{x}_{f,1} = \psi(\dot{y}_{0,1})$ first point;

- Stop if $|\dot{x}_{f,1}| < \epsilon$, with ϵ the desired tolerance for this first approach;
- $step = 0.1 \times |\dot{x}_{f,1}|$ variable step to get the slope between these two points;
- $\dot{y}_{0,2} = (1 + step) \times \dot{y}_{0,1}$
- $\dot{x}_{f,2} = \psi(\dot{y}_{0,2})$ second point;
- $\dot{y}_{0,1} \leftarrow \dot{y}_{0,2} - \frac{\dot{x}_{f,2}}{step\ \dot{y}_{0,1}}(\dot{x}_{f,2} - \dot{x}_{f,1})$ update the initial $\dot{y}_{0,1}$ for the next iteration of the loop;

After this first approach to determine $\dot{y}_0$, the differential correction using the STM is used to refine the value of $\dot{y}_0$. Once it is determined with precision, the whole orbit is fixed given a certain position of the asteroids. At the next time step they will be further apart, so the previously computed orbit is not accurate anymore and must be recalculated. X_0 can then be reused as initial guess instead of restarting from scratch, because for a small displacement of the primaries, the orbit should not be too much modified.

Because of the time-varying rotation velocity of the asteroids, the only periodic orbit in their rotating frame is the circular orbit. Therefore an elliptical orbit cannot be designed in the rotating frame using this previous method. The natural next step is then to try the inertial frame, because ellipses are periodic in that frame. However, that means recomputing the orbit at each time step with the primaries rotating inside. And their motion cause too much perturbations on the spacecraft trajectory to allow it to stay on an orbit close enough to the asteroids.

Since the coasting orbit cannot be computed, another option would be a low-thrust orbit that could be used as a reference. In that case the process at each time step would be :

- getting X_{ref} the reference state at the last time step;
- getting the geometrical path to follow during the time step;
- finding the thrust vector minimizing the error between the path and the propagation of X_{ref};
- using the whole Direct Adaptive process : calculate e, $\dot{e}$, V, $\dot{V}$, then u, the thrust vector for the actual state;

This method is too long, especially since the first steps could be applied directly to the actual state X, and then render the last step unnecessary.

Therefore the overall implementation follows an Indirect Adaptive Control scheme composed of three different blocks. The controller computes the thrust vector based on the reference path to follow and the current state, its precise functioning is described in subsection 4.4. The plant propagates the state a time step ahead using the Three Body Equations detailed in 4.2. The estimator refines the accuracy of the state using measurements as explained in subsection 4.3

The scheme described previously corresponds to a Self-Tuning Controller (STC) as defined in Lavretsky [25]. The main issue of this scheme is that its bedrock is the Certainty Equivalence Principle : the control u is computed from the estimates as if they were true. This happens because Controller and Estimator are two different blocks as can be seen on Figure 8 .

We have seen in 2.2.1 that to ensure the convergence of the parameters to their true values, the input signal must be

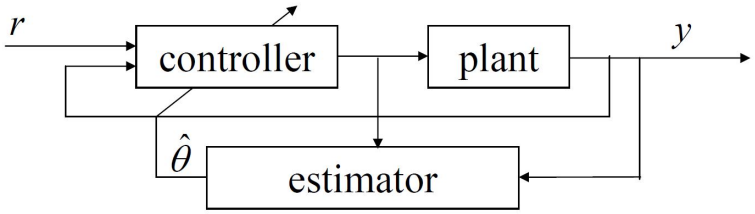

Fig. 8 Self-Tuning Controller (from Lavretsky [25])

rich enough, i.e. be persistently excited. This numerical condition can be checked during the propagation.

4.2. Restricted Three Body Problem Equations

In the usual studies of the Three Body Problem (3BP) the primaries are one celestial body and one of its satellite, the third body being the spacecraft whose trajectory is to be described. The most commonly studied 3BP is the Circular Restricted Three Body Problem (CR3BP), in which the smaller primary has a circular orbit around the other body. Almost all the literature dealing with a more global case than this simplified one dates back to the 1960s Szebehely [45]. The study of a contact binary asteroid that starts splitting does not fit in the CR3BP case, because the distance between these primaries is not constant and the rotation of the whole system is also time-varying. Thus, none of the usual normalization of the CR3BP can be used. For this reason all the calculations are run with the International System units.

The frame used for the calculations is the rotating frame with a time-varying rotation velocity Ω that brings all three rotating acceleration terms : the centrifugal, Euler and Coriolis forces.

The state vector is a 13-components vector $\mathbf{X}$ containing the six usual coordinates of the spacecraft plus the distance between the primaries d and their splitting velocity $\dot{d}$, accompanied by θ the angle between the inertial reference frame and the rotating one. The 4 following components are constant parameters to be estimated: the mass ratio of the asteroids μ, their normalized moment of inertia I_n, the initial rotating velocity of the asteroid Ω_0 and the initial distance between the center of mass of the two lobes d_0.

$$\mathbf{X} = [x,\ y,\ z,\ d,\ \dot{x},\ \dot{y},\ \dot{z},\ \dot{d},\ \theta,\ \mu,\ \Omega_0,\ d_0,\ I_n]^T \tag{11}$$

Since the relevant frame is rotating with respect to the inertial one, the forces considered are the rotating acceleration terms, the control thrust $\overrightarrow{u}$ and the gravitational attraction of the two primaries on the spacecraft. The latter is too light to affect the asteroids' motion.

$$m\overrightarrow{a} = \overrightarrow{F_{G1}} + \overrightarrow{F_{G2}} - 2m\overrightarrow{\Omega} \times \overrightarrow{v} - m\overrightarrow{\Omega} \times (\overrightarrow{\Omega} \times \overrightarrow{r}) - m\frac{d\overrightarrow{\Omega}}{dt} \times \overrightarrow{r} + \overrightarrow{u} \tag{12}$$

Equation 12 can be written projected on the axes of the rotating frame $(\overrightarrow{x}, \overrightarrow{y}, \overrightarrow{z})$ to obtain the traditional CR3BP

equations of motion 13

$$\begin{aligned}
\ddot{x} - 2\Omega\dot{y} - \Omega^2 x &= -\frac{Gm_1 d_1}{r_1^3} - \frac{Gm_2 d_2}{r_2^3} + \frac{u_x}{m}, \\
\ddot{y} + 2\Omega\dot{x} - \Omega^2 y &= -\frac{Gm_1 y}{r_1^3} - \frac{Gm_2 y}{r_2^3} + \frac{u_y}{m}, \\
\ddot{z} &= -\frac{Gm_1 z}{r_1^3} - \frac{Gm_2 z}{r_2^3} + \frac{u_z}{m}.
\end{aligned} \tag{13}$$

After some calculations, eq. (2) and eq. (13) can be gathered using the 13-components vector formulation :

$$\dot{\mathbf{X}} = \mathbf{f}(\mathbf{X}, \mathbf{u}) = \begin{bmatrix}
\dot{x} \\ \dot{y} \\ \dot{z} \\ \dot{d} \\
-G\frac{m_1 d_1}{r_1^3} - G\frac{m_2 d_2}{r_2^3} + \frac{u_x}{m} + x\Omega^2 + 2\dot{y}\Omega + y\dot{\Omega} \\
-G\frac{m_1 y}{r_1^3} - G\frac{m_2 y}{r_2^3} + \frac{u_y}{m} + y\Omega^2 - 2\dot{x}\Omega - x\dot{\Omega} \\
-G\frac{m_1 z}{r_1^3} - G\frac{m_2 z}{r_2^3} + \frac{u_z}{m} \\
d\Omega^2 - G\frac{(m_1+m_2)}{d^2} \\
\Omega \\ 0 \\ 0 \\ 0 \\ 0
\end{bmatrix} \quad with \quad \Omega(d) = \Omega_0 \left(\frac{I_n + \mu(1-\mu)d_0^2}{I_n + \mu(1-\mu)d^2} \right) \tag{14}$$

with $d_1 = x + \mu d$ and $d_2 = x - (1-\mu)d$ $r_1 = \sqrt{d_1^2 + y^2 + z^2}$ and $r_2 = \sqrt{d_2^2 + y^2 + z^2}$

The Jacobian of $\mathbf{f}$ can then be calculated :

$$\mathbf{F} = \frac{\partial \mathbf{f}}{\partial \mathbf{X}} = \left[\begin{array}{c|c|c|c}
0_{4\times4} & I_{4\times4} & 0_{4\times1} & 0_{4\times4} \\ \hline
dF_{4\times4} & \Omega_{4\times4} & 0_{4\times1} & dCST_{4\times4} \\ \hline
0_{1\times4} & 0_{1\times4} & 0_{1\times1} & 0_{1\times4} \\ \hline
0_{4\times4} & 0_{4\times4} & 0_{4\times1} & 0_{4\times4}
\end{array}\right]$$

All the details are in Appendix A 6. The shape of the top left 8×8 sub-matrix of $\mathbf{F}$ is very similar to the one used in the CR3BP to propagate the State Transition Matrix (STM); it is serving the same purpose here. The addition of the constants results in the addition of the six last columns and rows which are almost all empty.

4.3. Extended Kalman Filter

Since the spacecraft can only get access to its state through noisy measurements, an algorithm to refine those values and acquire accurate data is required. To fulfill this task an Extended Kalman Filter (EKF) with discrete time

measurements has been implemented. The first step in an estimation process is to determine if the system is observable. Indeed, if this is not the case, then another set of independent and observable variables must be selected. Since our system is nonlinear, the traditional observation matrix of linear systems is not valid. Song and Grizzle [46] establish the observability conditions for a nonlinear discrete-time system, by building a local asymptotic observer. Let consider the following system, and its 'noisy' version:

$$\begin{aligned} x_{k+1} &= f_D(x_k, u_k) & \qquad z_{k+1} &= f_D(z_k, u_k) + Qw_k \\ y_k &= h(x_k, u_k) & \qquad \zeta_k &= h(z_k, u_k) + Rv_k \end{aligned} \tag{15}$$

We will need the Jacobians of the system: $A_D = \frac{\partial f_D}{\partial x}$ and $C = \frac{\partial h}{\partial x}$ and evaluate them at different times. The local asymptotic observer is then:

$$O_D(k, n-1) = \begin{bmatrix} C(x^-_{k-n+1}) \\ C(x^-_{k-n+2})A_D(x_{k-n+1}) \\ \vdots \\ C(x^-_k)A_D(x^-_{k-1})...A_D(x^-_{k-n+1}) \end{bmatrix} \tag{16}$$

We can then check the usual observability condition: if $rank(O) = n$, then the system is locally observable. Our system being continuous, a small variation of this method has been implemented. We will denote with a C the continuous quantities, and with a D those from the discrete case. The propagation equation are then $x_{k+1} = f_D(x_k)$ and $\dot{x} = f_C(x)$. At the first order,

$$f_C(x_k) = \dot{x}_k \simeq \frac{x_{k+1} - x_k}{dt} = \frac{f_D(x_k) - x_k}{dt} \qquad so \qquad f_D(x_k) \simeq x_k + f_C(x_k)dt \tag{17}$$

Then we can calculate the Jacobians :

$$A_D(x_k) \;=\; \frac{\partial f_D}{\partial x}(x_k) \;=\; I \;+\; \frac{\partial f_C}{\partial x}(x_k)\, dt \tag{18}$$

The observation equation are unchanged so $C_D = C_C$. We can then plug eq. (18) in eq. (16) to obtain the continuous asymptotic observer O_C

After implementation of O_C, the system is found to be always asymptotically locally observable. Yet this concern the locally linearized system. The global observability of the nonlinear system is more difficult to assess, and out of the scope of this thesis.

With the notations used in the previous section 4.2, X is the estimated state and Y the actual state, f is the state transition function, F its Jacobian, Z the observation and u the thrust. The other matrices come from the EKF and are respectively : R the covariance matrix of the measuring noise $V(t)$, Q the covariance matrix of the process noise $W(t)$, h

the observation function and H its Jacobian, G the gain matrix, P is the prediction error and I the identity matrix of the appropriate size.

$$\begin{array}{lll} MODEL & PREDICT & UPDATE \\ \dot{Y}(t) = f\Big(Y(t),\ u(t)\Big) + W(t) & \dot{X}(t) = f\Big(X(t),\ u(t)\Big) & G = PH^t(HPH^t + R)^{-1} \\ Z = h(Y) + V(t) & \dot{P}(t) = F(t)P(t) + P(t)F^t(t) + Q & X = X^- + G(Z - h(X^-)) \\ & & P = (I - GH)P \end{array} \tag{19}$$

The observation Z is the information received by the spacecraft. Z is composed of two 6-components position-velocity vectors between the spacecraft and both asteroids. The sensors measure distance and speed in the inertial frame based on fixed stars. For simplicity's sake, it has been assumed that the frame of the asteroids rotates around the Z-axis of the inertial frame. This rotations is parametrized by the angle θ and its time derivative $\frac{d\theta}{dt} = \Omega(t)$. So the observation function transforms a 13-components rotating vector into two 6-components inertial vectors :

$$\mathbf{h}(\mathbf{X}) = \left[\begin{array}{c} cos(\theta)(x + \mu d) - sin(\theta)y \\ sin(\theta)(x + \mu d) + cos(\theta)y \\ z \\ -\Omega\big(sin(\theta)(x + \mu d) + cos(\theta)y\big) + cos(\theta)(\dot{x} + \mu\dot{d}) - sin(\theta)\dot{y} \\ \Omega\big(cos(\theta)(x + \mu d) - sin(\theta)y\big) + sin(\theta)(\dot{x} + \mu\dot{d}) + cos(\theta)\dot{y} \\ \dot{z} \\ \hline cos(\theta)(x - (1-\mu)d) - sin(\theta)y \\ sin(\theta)(x - (1-\mu)d) + cos(\theta)y \\ z \\ -\Omega\big(sin(\theta)(x - (1-\mu)d) + cos(\theta)y\big) + cos(\theta)(\dot{x} - (1-\mu)\dot{d}) - sin(\theta)\dot{y} \\ \Omega\big(cos(\theta)(x - (1-\mu)d) - sin(\theta)y\big) + cos(\theta)(\dot{x} - (1-\mu)\dot{d}) + cos(\theta)\dot{y} \\ \dot{z} \end{array}\right] \tag{20}$$

The observation has to be built from the state X to follow the EKF process, and that is the reason of the presence of θ in the state vector. The detailed calculations of the Jacobian $H = \frac{\partial h}{\partial X}$ can be found in Appendix section 6.

Concerning the prediction error matrix P, several improvements have been implemented following the advice from Schneider and Georgakis [23]. First comes the choice of the initial value P_0. The prediction matrix contains values between zero and one, based on the confidence on the accuracy of the estimates; 0 being for a perfect estimate and 1 for a poor estimation. The best initialization is to take $P_0 = (X_0 - Y_0)^T \cdot (X_0 - Y_0)$ because it directly quantifies the precision of the estimate. However, the actual initial state Y_0 must be available, which is not the case here. A simple option would be to initialize P_0 as a matrix full of ones, then no over-confidence is given to any estimate. Yet assigning

the worst initialization is not a good idea, since some information is available concerning the initial state. Indeed, the approximate size of the zone around the estimate where the true value lies is usually known. The initial state estimate X_0 is built from the true one using $X_0 = D \cdot Y_0$, with D a diagonal matrix which terms follow a normal distribution of average one and of standard deviation $\sigma = 0.07$. It is reasonable to assume this σ known since it characterizes the previously mentioned size of the zone. And then $P_0 = (2\sigma X_0)^T \cdot (2\sigma X_0)$.
The second improvement is a more robust update equation for P using the Joseph stabilized version :
$P = (I - GH)P(I - GH)^T + GRG^T$

4.4. Controller

The controller is the part of the process that designs the control input, for the current position to track a certain reference described in the mission requirements. In this paper the spacecraft aims at orbiting elliptically around the asteroids. The controller can be designed along two main philosophies : Path Following or Trajectory Tracking.

A path is a list of positions, while a trajectory also has a timing law associated, i.e. a velocity and acceleration at each position. Yet having both of them available on the desired trajectory is not always the case. Moreover for a specific mission or due to a very unusual asteroid shape, the orbit may need to be specifically designed for this case and to be more complicated than a circle or an ellipse. In such a case, the propagation of the desired orbit can be a lot more difficult, as detailed in section 4.1, especially to obtain in real-time the desired acceleration and velocity at a certain position.

4.4.1. Path Following

Thus the solution is to implement a Path Following strategy, using a slight variation of the method developed in [24]. The usual method is to add an extra control parameter in order to describe the timing law which parametrizes the position to track on the desired path, transforming path following into trajectory tracking. And then at each time step an optimization problem must be solved to find the best thrust and timing law for the next step. In a Trajectory Tracking context a PID controller would be used to stabilize the trajectory close to the desired path. Yet in the Path Following case the velocity and acceleration on the path are not available so we cannot implement a Feedback Linearization algorithm with a PID controller. Instead, the thrust computation algorithm has access to a longer time horizon, to be able to anticipate and prevent divergences. This anticipation helps preventing overshoot and oscillations which usually happen when trying to minimize the distance to a path when looking only one time step ahead.

The timing-law is also an extra parameter to optimize but the insights about its value are difficult to acquire. Thus a simpler method has been implemented, the position to track is just the point on the desired path that is the closest to the current position.

At each time step the best thrust to apply to the spacecraft is calculated. For a predetermined thrust, the trajectory is

propagated for a number PH of time steps δt, PH being the Prediction Horizon. And then the integral error of this trajectory with respect to the desired path is calculated following the method described in [47]. This error is considered as a cost to minimize and this optimization problem is to be solved at each time step in order to determine the best thrust vector.

The minimization problem to solve is finding the thrust vector u in order to minimize the error. u is bounded with u_{inf} and u_{sup}, which are characteristics of the thrust system.

$$\min_{\forall t\ u_{inf}\ \leq u(t)\ \leq u_{sup}} \int_{t_0}^{t_0+PH} ||X\big(t, u(t)\big) - X_{ref}(t)||\ dt \tag{21}$$

The implementation being not continuous, the thrust is constant per time step, so eq. (21) has to be modified. A rolling horizon method is implemented with four different time scales, as described in fig. 9.

- The Scheduling Horizon SH is the total time range of the mission;
- The Prediction Horizon PH is subdivided into N Control Horizons : $PH = N \times CH$. At each time step the state is propagated over PH for the system to anticipate and provide an appropriate answer;
- Over the Control Horizon CH, the thrust is considered constant. It can be divided into H time steps δt because the thrust does not vary too much over just one time step. So $CH = H \times \delta t$. The thrust will actually change at the next time step, but this process allows to look further ahead for almost the same computation time;
- The time step δt is the smallest time scale, it corresponds to the step of the iterations of the state propagation;

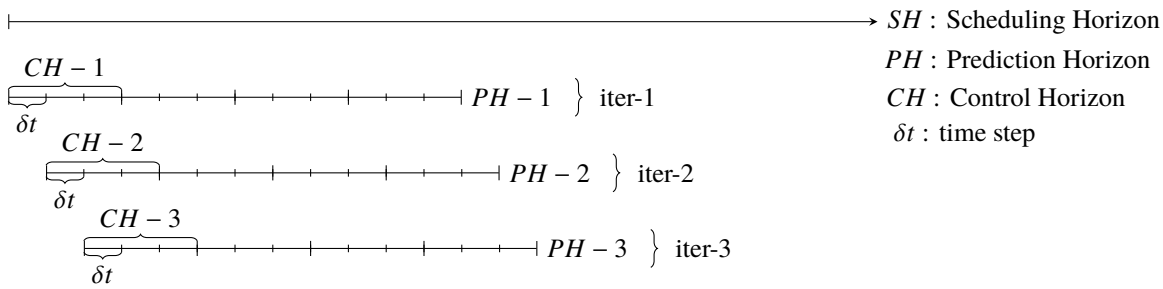

Fig. 9 Rolling Horizon with $N = 4$ and $H = 3$

To sum up, there are two design parameters for this rolling horizon scheme : the integers N and H. Their values will be optimized in the section 5. We can now update eq. (21) with the rolling horizon to finally obtain eq. (22)

$$\min_{\substack{u_{inf} \leq u_1 \leq u_{sup} \\ \vdots \\ u_{inf} \leq u_N \leq u_{sup}}} \sum_{k=1}^{N} \int_{t_0+(k-1)CH}^{t_0+kCH} ||X(t, u_k) - X_{ref}(t)||\ dt \tag{22}$$

In the current implementation only the elliptical and circular orbits cases have been considered, leading to a specific

algorithm to calculate the distance between the spacecraft and the closest point on the path. But more general algorithm exist [48] and allow any type of orbit to be followed.

A common issue arising from this algorithm, is that the direction in which to follow the path is not prescribed, and thus the minimization can also lead to an abrupt turn-around. To prevent this, a simple sign check of the cross product between the position vectors at the beginning and at the end of the time Horizon can be performed, and a higher cost given to the unwanted direction of propagation.

4.4.2. Trajectory Tracking

Before implementing the Path Following strategy for the reasons detailed previously, we started with a trajectory tracking approach. This method is able to successfully follow a circular orbit, but does not work for elliptical orbits. That is the reason why we had to abandon it.

We adopted the tracking strategy described in [49]. Our state equations fit into the dynamical model described in the reference:

$$B(q)\ddot{q} + c(q,\dot{q}) + g(q) + \text{friction model} = B(q)\ddot{q} + n(q,\dot{q}) = u \tag{23}$$

with q the state vector and u the control input. The objective is to follow a desired trajectory $q_d(t), t \in [0,T]$ denoted with a subscript d. q_d must also be at least twice differentiable. The model estimates are denoted with a hat $\hat{}$. And so the desired system is : $\hat{u}_d = \hat{B}(q_d)\ddot{q}_d + \hat{n}(q_d,\dot{q}_d)$. Several of the command laws have been tried :

- a feedback linearization with a Proportional Derivative (PD) controller:
  $u = \hat{B}(q)\left[\ddot{q}_d + K_p(q_d - q) + K_d(\dot{q}_d - \dot{q})\right] + \hat{n}(q,\dot{q})$
- a feedback linearization coupled with a Proportional Integral Derivative (PID) controller:
  $u = \hat{B}(q)\left[\ddot{q}_d + K_p(q_d - q) + K_i\int(q_d - q)dt\right] + K_d(\dot{q}_d - \dot{q}) + \hat{n}(q,\dot{q})$
- and even a feedback linearization with a Cube PID controller based on [50]: $u = \hat{B}(q)\Big[\ddot{q}_d + K_p(q_d - q) + K_i\int(q_d - q)dt + K_d(\dot{q}_d - \dot{q}) + K_{pc}(q_d - q)^3 + K_{ic}\int(q_d - q)^3dt + K_{dc}(\dot{q}_d - \dot{q})^3\Big] + \hat{n}(q,\dot{q})$

The challenge here was to find proper values for the gains K_p, K_i and K_d. A two-step method was implemented: first a grid search to reduce the interval of possible values, and then to refine the search a Particle Swarm Optimization algorithm (PSO) was used, following the same method as in [51].

During the gains optimization the cost function to minimize has been selected to be the integral error with respect to the desired orbit:

$$cost = \int_0^T \Big(|x_d(t) - x(t)| + |y_d(t) - y(t)| + |z_d(t) - z(t)|\Big)dt \tag{24}$$

If the trajectory diverges of more than a set distance d_{cut} from the reference one, then the cost is set to infinity. Even if PSO is a perfectly sufficient optimization algorithm, the prior Grid Search is necessary. Indeed, for some values of

the gains, the controller is not robust and thus the associated trajectory will diverge in most cases. But if the noise along the propagation is well-behaved then the trajectory can converge, and this happens usually with a low probability. Since during the Grid Search each combination of gains is tested only once, such a case will be eliminated due to its highly probable divergence. On the contrary, the stochastic component of PSO can test close gains combination a great number of time and then manage to find an unstable minimum. During the tests it occurred that these minimum had extremely low costs. Therefore is the Grid Search is not performed before PSO to restrain the test field to stable values, the minimum found by PSO is likely to be unstable and thus useless. To precise the meaning of an unstable trajectory, as previously employed would be that by launching several times the same computations, with the same gains, the results are always different due to the process and measure noise.

Another drawback of the trajectory tracking is that the gains must be recalculated for each new orbit, and their optimization is computationally expensive.

5. Results

5.1. Initialization

The method developed in this thesis is applicable to any contact binary asteroid system. To obtain realistic numerical values our algorithm has been applied to three actual asteroids : Castalia, Kleopatra and 1996 HW1. These three test cases use the values gathered in the Table 1 for the asteroids model.

The spacecraft model is close to the orbiter Rosetta that performed a similar mission. The orbit has been chosen big enough for the spacecraft to complete a whole orbit after the splitting, while the final distance between the asteroids becomes comparable to the orbit size.

Table 3 Value of the main parameters for the test case

Asteroid parameter	Orbit	Value	Spacecraft	Value	Algorithm	Value
d_0 : distance between centers	Semi major axis	$10 \times d_0$	m_{SC}	$3 \times 10^3\ kg$	T_{step}	$T/400$
T : asteroids' rotation period	Eccentricity	0.6	Max thrust	$0.1\ N$	H	2
					N	5
					d_{CUT}	$10\ km$

T_{step} is the time step for the calculations. It is chosen as a fraction of the period for scale purposes. Since the asteroids are splitting, the total moment of inertia increases, so to conserve the angular momentum their rotating velocity decreases, thus the period T increases. Therefore to prevent the number of time step to grow too much, their size is updated with T. d_{CUT} is the maximal distance allowed between the actual trajectory and the desired one. If the error reach this limit, then the calculations are stopped and this case is considered as a failure.

The Extended Kalman filter also requires several initialization. We already discussed how to set the initial value of the prediction error matrix $P_0 = (2\sigma X_0)^T \cdot (2\sigma X_0)$, with $\sigma = 0.07$. As for the covariance matrix R of the measuring noise, its values were chosen constant throughout all the experiments. The measures are composed of two 6-components position-velocity vectors between the spacecraft and each asteroids. Therefore, R is a 12×12 diagonal matrix. Elements 1 to 3 and 7 to 9 are associated with the distance measures, while the others are related to the relative velocity measures. Thus, only two scalar values are sufficient to define the whole R matrix. In the simulations, we chose $R(1,1) = 10^{-2}\ km$ and $R(4,4) = 10^{-4}\ km/s$

The initialization of the covariance matrix Q of the process noise is more tricky. Indeed Q is constant and its value is crucial to the success of the estimation process. Valappil and Georgakis [52] describes that if the value of Q is too low with respect to its nominal value, then the EKF is overconfident in the estimate and ignore the measurements. If Q is too high, then the estimates will rely too much on the measures and become noisy. So far, the value of Q has then been selected by trial and error, but we are working on an automated process.

5.2. First results

The first step of the process is to prove that a control law is actually needed, because the natural dynamics of the spacecraft would not maintain it on orbit around the splitting asteroids. For the asteroid Castalia, when no thrust is applied the spacecraft flies away as can be seen in Figure 10. The reference trajectory is red, while the actual one is blue. The same divergence happens for all of our test cases. The spacecraft initially has the velocity required to stay on the specified elliptic orbit around one central body of mass m_{tot}. When the asteroids start to split, this assumption does not hold anymore and the gravitational force acting on the spacecraft decreases, it has therefore a velocity too high to stay on the initial orbit and will then diverge.

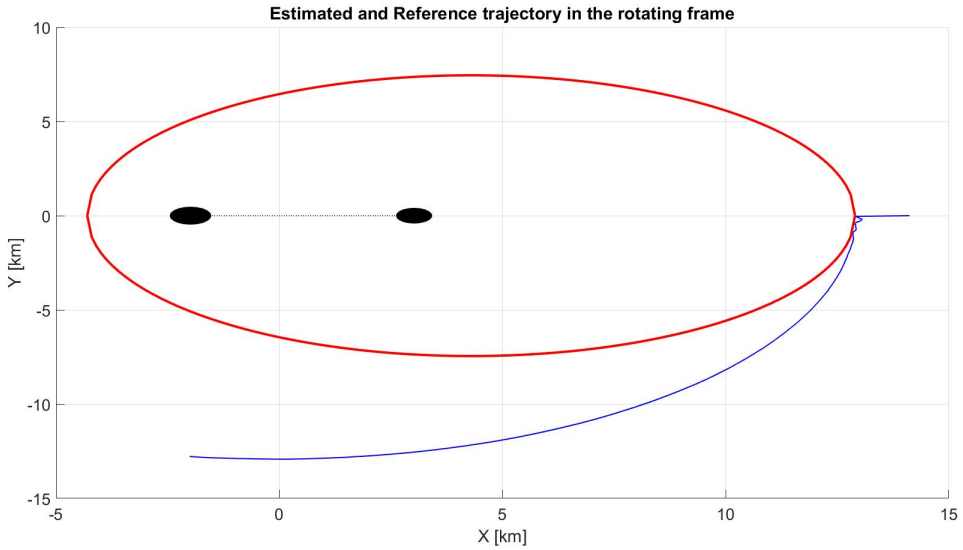

Fig. 10 Free propagation around asteroid Castalia in the rotating frame

When the spacecraft is allowed to use thrust control and the path following method described in section 4.4, two parameters must be chosen by the user N and H. They both are positive integers, so even without any knowledge of their role, the first value tested is $N = H = 1$. However, as can be seen on fig. 11, the result is not optimal. We will study in more details the role of these two parameters in section 5.3, and how to optimize their choice. Indeed, they play a crucial role in the precision of the path following algorithm and also in the total computation time of the overall method.

The asteroids' motion is not affected by the spacecraft and its controller. So we can already access their splitting distance d in section 5.2. The curve is not as smooth as expected because of the white process noise introduced in our equations of motion to represent the unmodeled dynamics.

We will use two scales to represent our data: either the time or the angle of the spacecraft on its orbit, depending on which is the most appropriate for the data to plot. They can both be used as X-axis without ambiguity, because when the spacecraft does not turn around, we can build a bijection between these two parameters, as section 5.2 proves it.

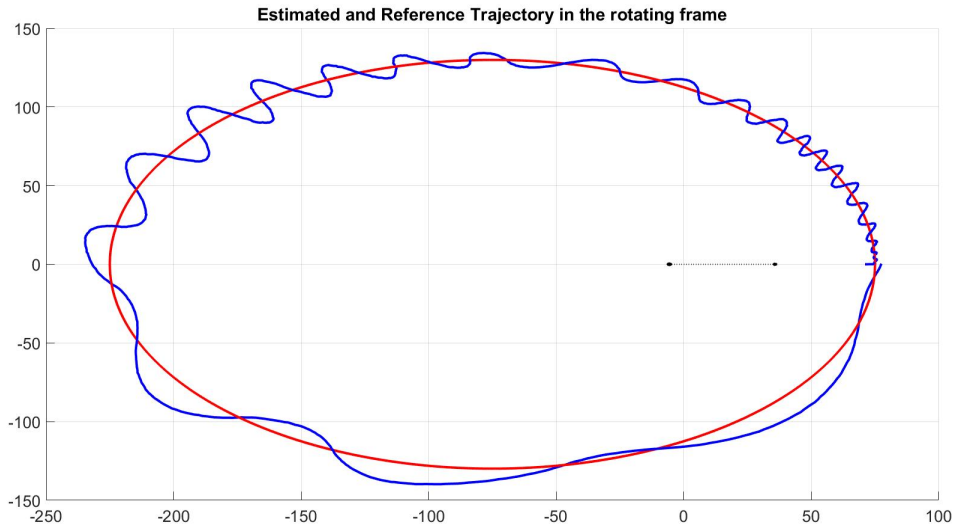

Fig. 11 Orbit for $H = N = 1$

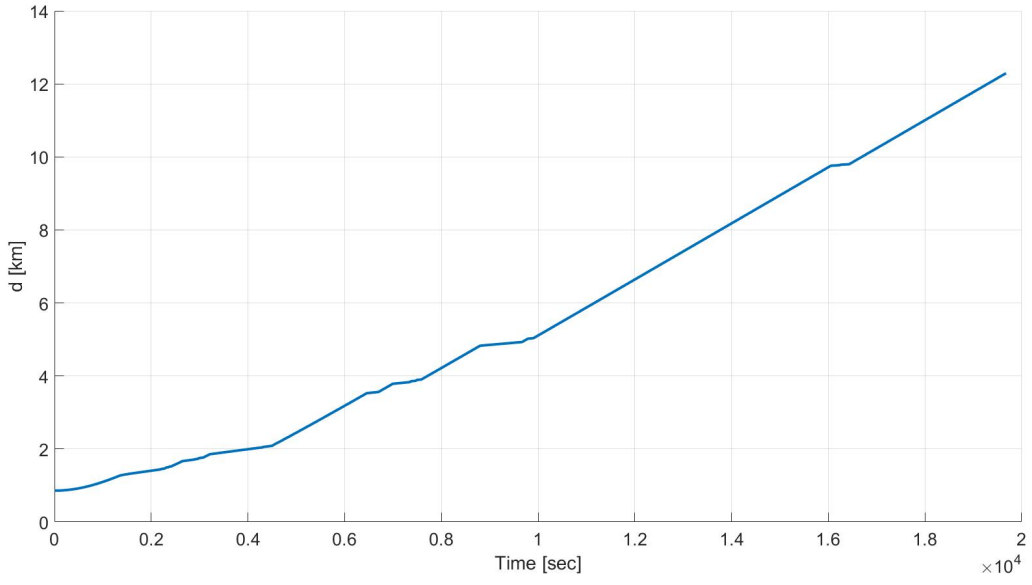

Fig. 12 Evolution of the distance between the lobes of the asteroid Castalia

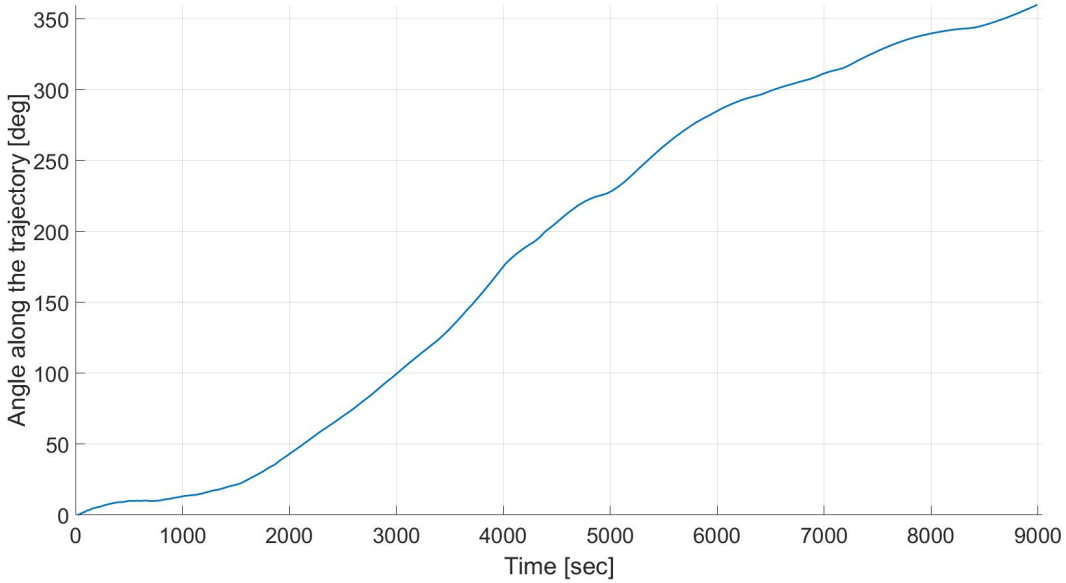

Fig. 13 Angle of the spacecraft on its orbit around the asteroid

5.3. Optimization of the parameters of the tracking algorithm

Two parameters of the controller must be chosen by the user: H and N as they are defined in section 4.4. They are responsible for the anticipation of the controller. If $H \times N$ is too small then the controller cannot anticipate trajectory modifications and an overshoot phenomenon take place, leading to numerous unwanted oscillations as can be seen in fig. 11.

Now we will study the effect of the parameter N, with H fixed at the value 2. This choice for the value of H will be justified later. We computed the orbit around the asteroid Castalia for $N \in \{1,\ 2,\ 3,\ 4,\ 5,\ 6\}$ in respectively fig. 14, 15 16, 17, 18 and 19. We can remark that the initialization of the estimated state is noisy and therefore out of the desired path, but the EKF corrects it in a few iterations. When N is too small the controller cannot anticipate enough and we can see the oscillations around the desired orbit. These oscillations decrease in amplitude with the increase of N until $N = 4$ where the progress are less striking than before.

We can remark that the initialization of the estimated state is noisy and therefore out of the desired path, but the EKF corrects it in a few iterations. The starting point is at the right extremity of the ellipse, which is in fact the apogee of the orbit. The primaries start around $(0, 0)$ and the spacecraft at $(12, 0)$. The orbit is propagated for a complete revolution, it stops when the spacecraft hits the positive X-axis again. The asteroids don't travel the same distance in the figures because the time required for the spacecraft to complete its orbit is not the same, it depends on the efficiency of the controller.

To measure the efficiency of the controller, we established a metric : $\epsilon = \int_{\phi=0}^{2\pi} ||\overrightarrow{X} - \overrightarrow{X_{des}}||\ d\phi$. ϵ is the integral

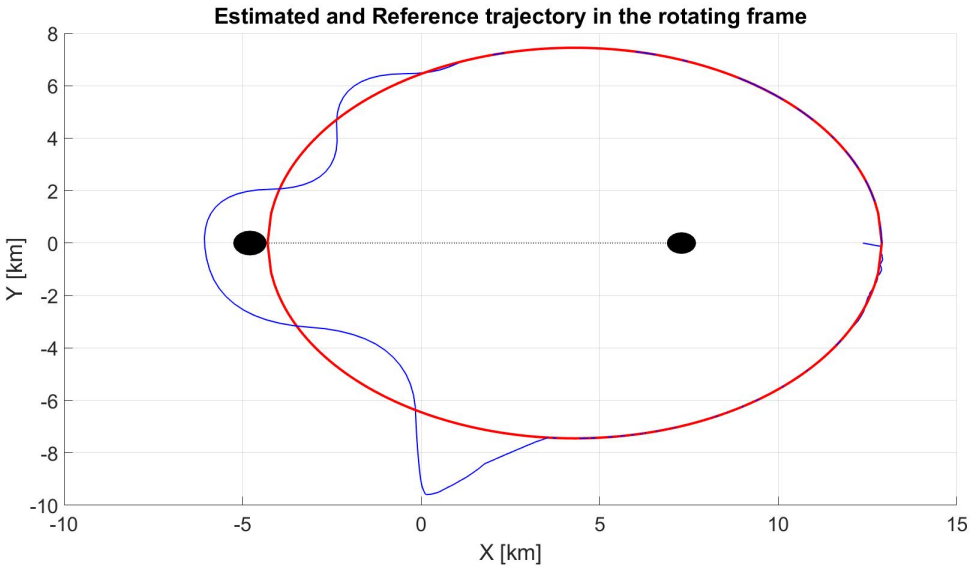

Fig. 14 Orbit around Castalia with $N = 1$ and $H = 2$

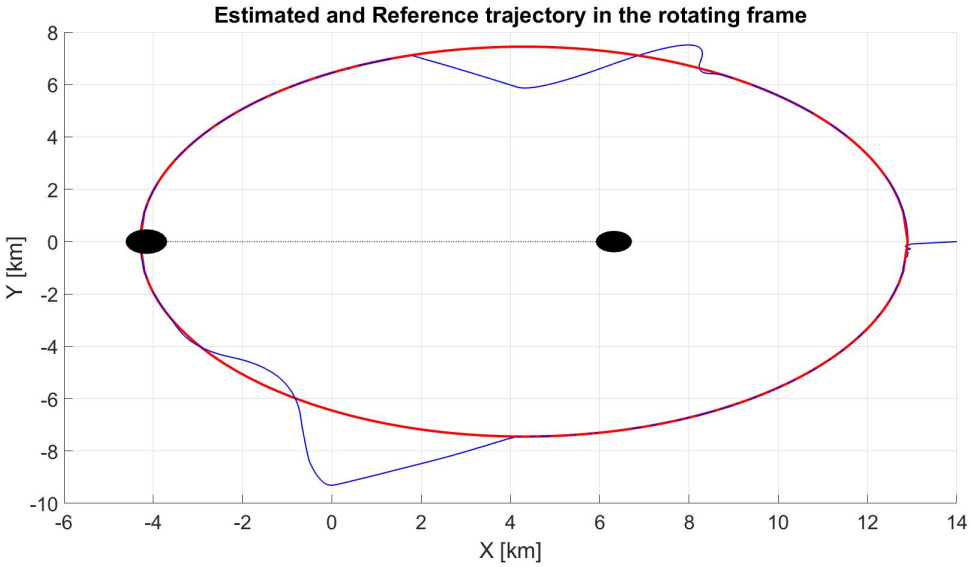

Fig. 15 Orbit around Castalia with $N = 2$ and $H = 2$

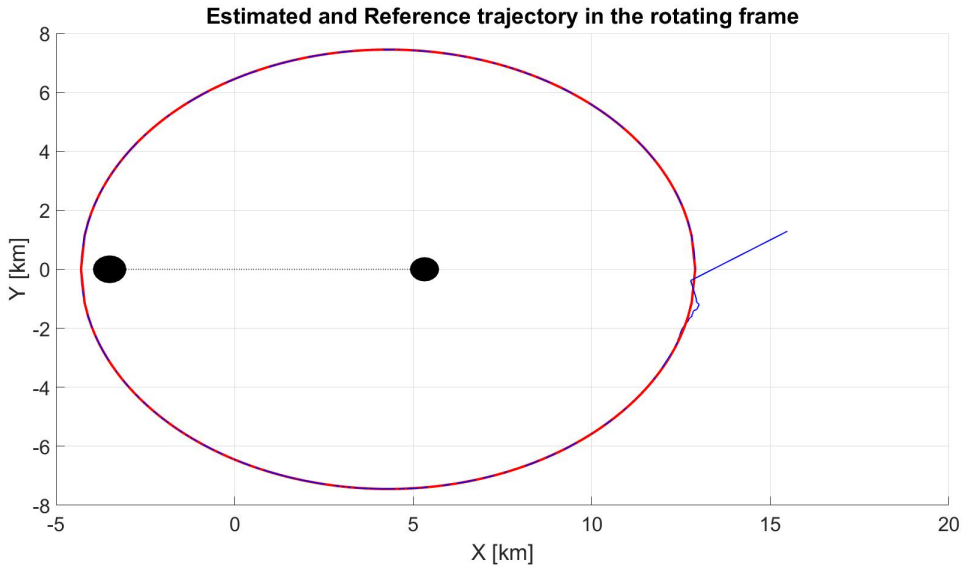

Fig. 16 Orbit around Castalia with $N = 3$ and $H = 2$

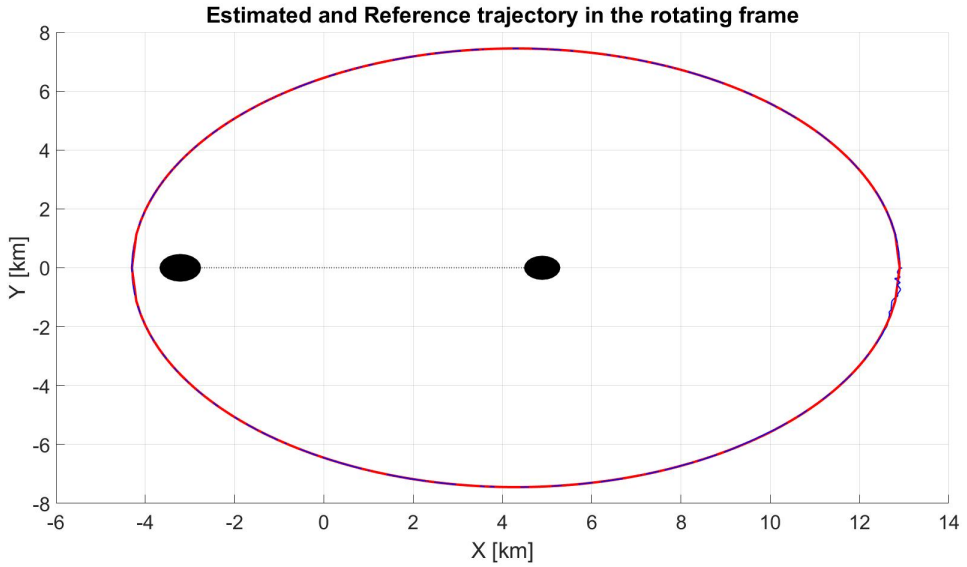

Fig. 17 Orbit around Castalia with $N = 4$ and $H = 2$

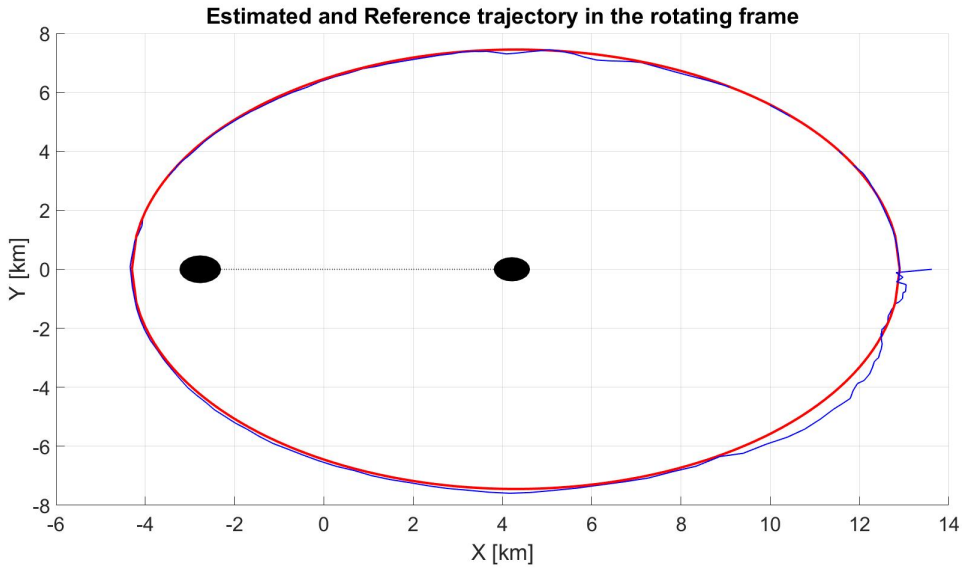

Fig. 18 Orbit around Castalia with $N = 5$ and $H = 2$

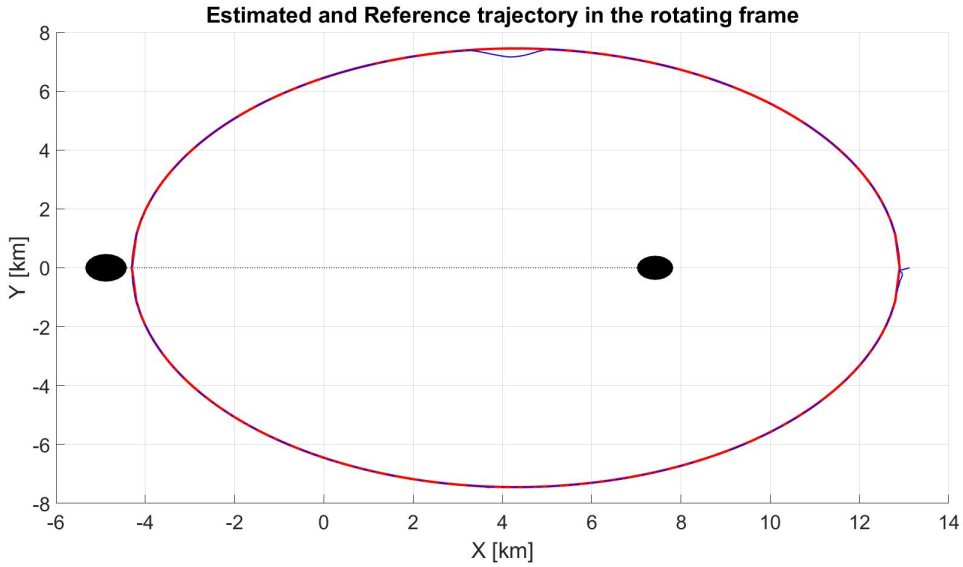

Fig. 19 Orbit around Castalia with $N = 6$ and $H = 2$

error over an orbit between the actual and desired positions. We assumed that between two time steps the position of the spacecraft is almost the same, thus the thrust vector to apply should also be the same. This assumption is reflected by H, which is the number of consecutive time steps over which the thrust is considered constant in the optimization process. It enables to drastically cut down the computation time for the same Prediction Horizon. fig. 20 shows that the assumption is valid for $H \in \{1, 2, 3\}$.

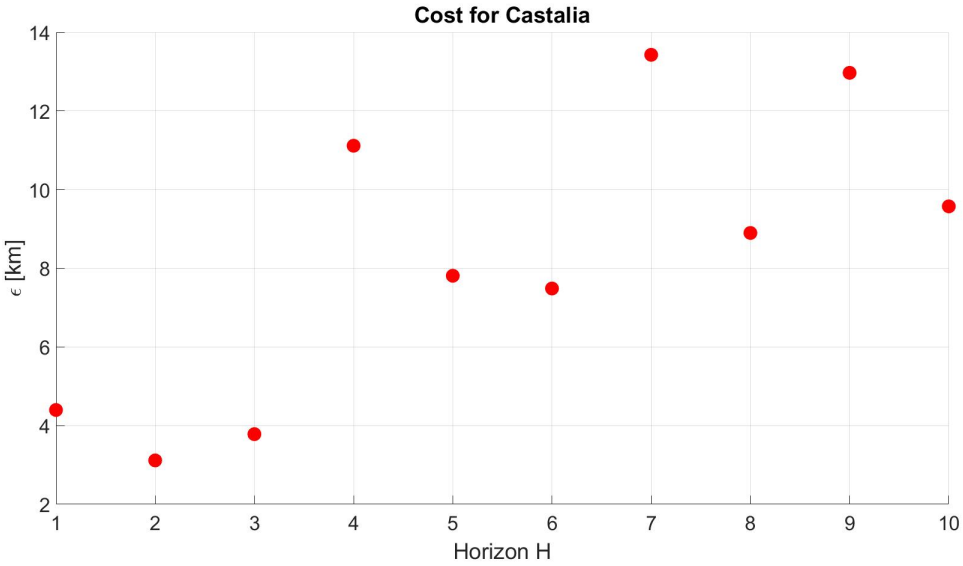

Fig. 20 Integral error ϵ as a function of H

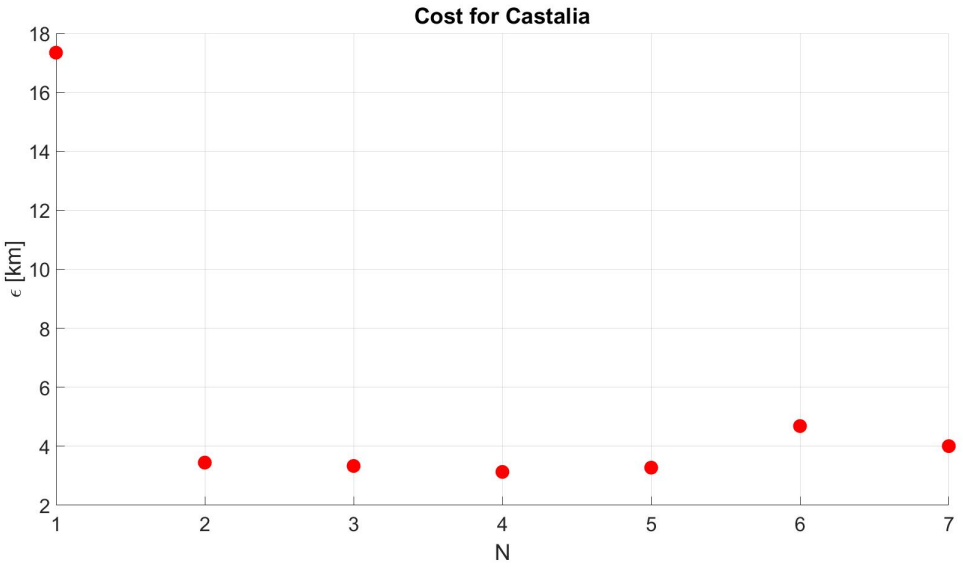

Fig. 21 Integral error ϵ as a function of N

On the other hand, the impact of N should be straightforward: increasing it expands the Prediction Horizon without making any assumption. Therefore, the higher N is, the better the accuracy should be. However, fig. 21 shows that for

$N \geqslant 2$ the accuracy is not really impacted, and we can also see not great improvements for $N \geqslant 4$ in fig. 17, 18, 19.

Another parameter giving an insight about the efficiency of the path following algorithm is the total impulse. This quantity is the time integral of the thrust needed by the spacecraft to stay on orbit. The time horizon enables the program to anticipate and prevent the waist of propellant. Therefore by increasing N and H the total impulse decreases, as can be seen in fig. 22.

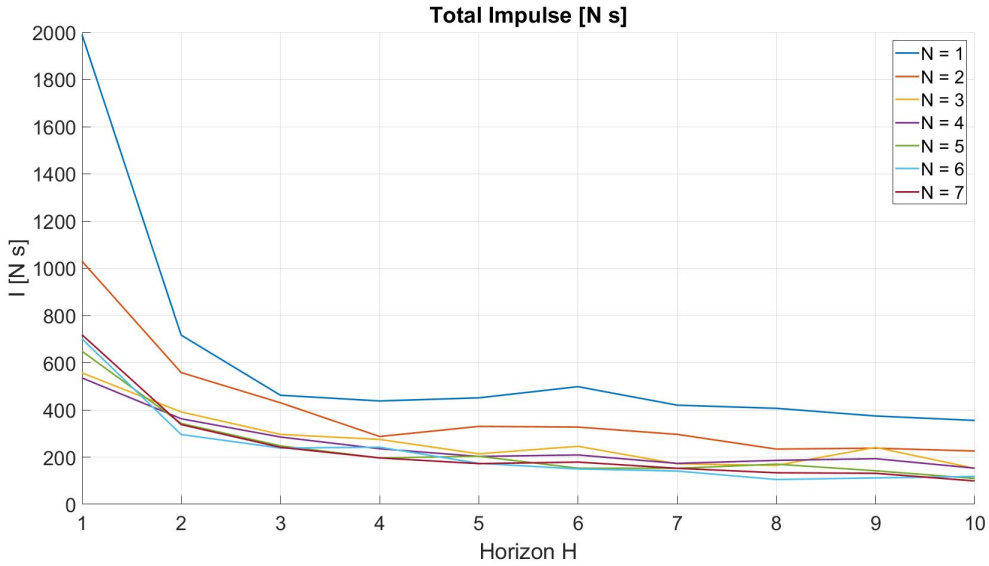

Fig. 22 Total impulse as function of N and H

Among the three main steps of the algorithm: thrust calculation, integration of the EOM and EKF, the one that requires the most computation time is the thrust calculation, because of the optimization problem to be solved. The computation time is highly dependent on the value of N chosen. Indeed, it directly determines how many 3D thrust vectors the optimizer has to determine. In fact, the dimension of the search space is $3 \times N$. Therefore, one could expect a linear growth of the computation time with N, but it is absolutely not the case, as can be seen in table 4. The reason is that the optimizer is the nonlinear MATLAB method $fmincon$.

Table 4 Computation time

$N = 1$	$N = 2$	$N = 3$	$N = 4$	$N = 5$	$N = 6$	$N = 7$
5 min	24 min	58 min	1 hr 56 min	3 hr 21 min	5 hr 24 min	7 hr 41 min

On the other hand, the computation time is almost not affected by the value of H, as shown in fig. 23. Indeed, increasing H increases the time interval over which the equations of motion are integrated, but this is negligible compared to the time consumed by the optimizer.

Therefore the determination of the parameter N results from a compromise between accuracy and computation time. If we want this program to run on real time in the spacecraft, then the time is constrained and will dictate the possible

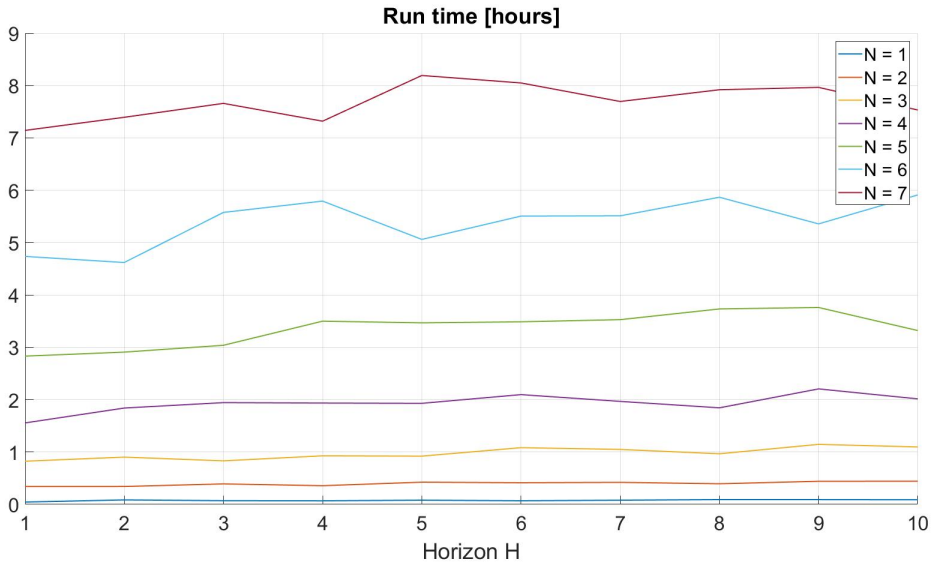

Fig. 23 Computation time as function of N and H

accuracy.

5.4. Parameters Convergence

We first need to ensure that the system is observable. A global nonlinear observability check is out of the scope of this thesis. Yet, a simple observability check on the locally linearized system is easy to implement and brings useful results. We implemented the method summarized by the two equations 15 and 18. $rank(O_D)$ is computed at each time step, and compared with the size of the state vector.

Initially, our state vector was: $X = [x,\ y,\ z,\ d,\ \dot{x},\ \dot{y},\ \dot{z},\ \dot{d},\ \theta,\ m_1,\ m_2,\ I_1,\ I_2,\ \Omega_0,\ d_0]$. This system is not observable: $rank(O_D) = 13 < length(X) = 15$. Indeed, in the equations of motion, the two moments of inertia of the asteroids I_1 and I_2, always appear together as $I_1 + I_2$ in the formula of Ω. Therefore, they could not be distinguished and needed to be combined together. We also normalized them by the total mass to eventually obtain a parameter I_n of magnitude closer to the other states.

The masses of each asteroids are also not observable together. Indeed, we have two distance measurements, but three parameters to describe their distance: d, m_1 and m_2, because their positions are linked through the mass ratio $\mu = \frac{m_2}{m_1+m_2}$: along the X-axis the position of m_1 is $-\mu d$, while the other is $(1-\mu)d$. Thus, to make the system observable we considered μ instead of $m_{1,2}$ in the state vector. So we reduced its length to 13 while maintaining the rank of the observability matrix, which is now full rank. The system is now locally observable.

We have seen in section 2.2.1 that one of the main point of the adaptive control implementation concerns the convergence of the estimates to their true values. We considered 13 parameters to estimate and grouped them together in our state vector $X = [x,\ y,\ z,\ d,\ \dot{x},\ \dot{y},\ \dot{z},\ \dot{d},\ \theta,\ \mu,\ \Omega_0,\ d_0,\ I_n]$. They have been estimated and compared to their

true values along the propagation.

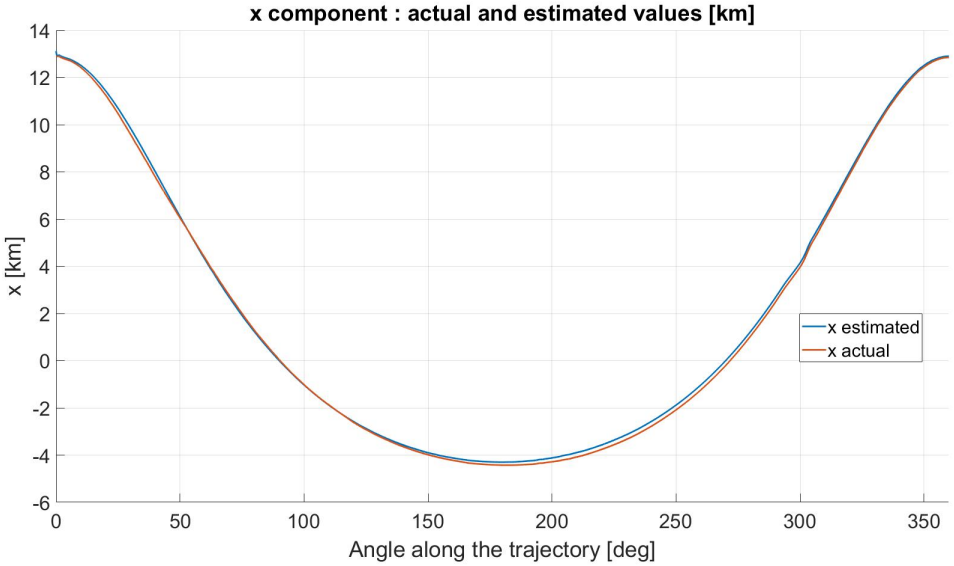

Fig. 24 Actual and estimated values of x

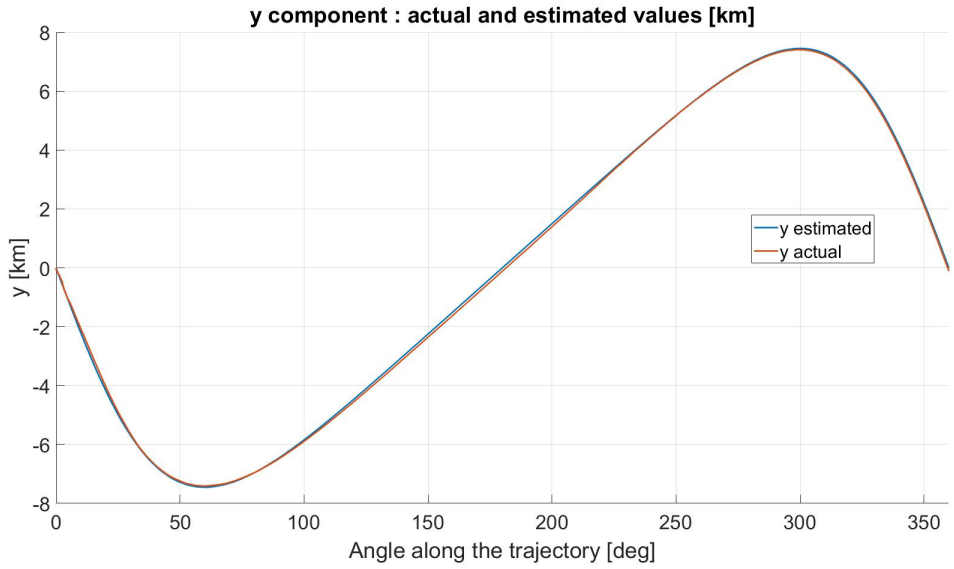

Fig. 25 Actual and estimated values of y

The x and y components have very similar roles in the equations of motion, and thus they converge together. This convergence takes place in most cases, because it is very straightforward to find x and y based on the observations of distance with respect to the asteroids. They are almost directly observable. The situation is exactly the same for $\dot{x}$, $\dot{y}$ and the velocity measures.

The third axis z is not considered like the two others in the observations h as one may remark in eq. (20). z and $\dot{z}$ are directly observable because the inertial frame in which the spacecraft takes its measurements has the same Z-axis as the

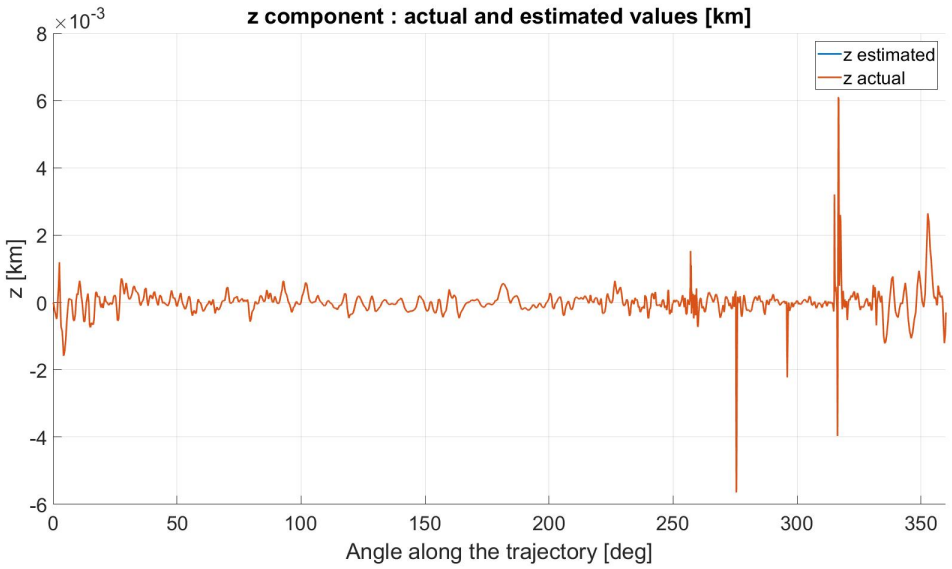

Fig. 26 Actual and estimated values of z

asteroids frame. This assumption simplifies the calculations, but can easily be discarded to render the problem more general without affecting the results. Since they are directly measured, the convergence error is sufficiently small that even the process noise is clearly visible in fig. 26

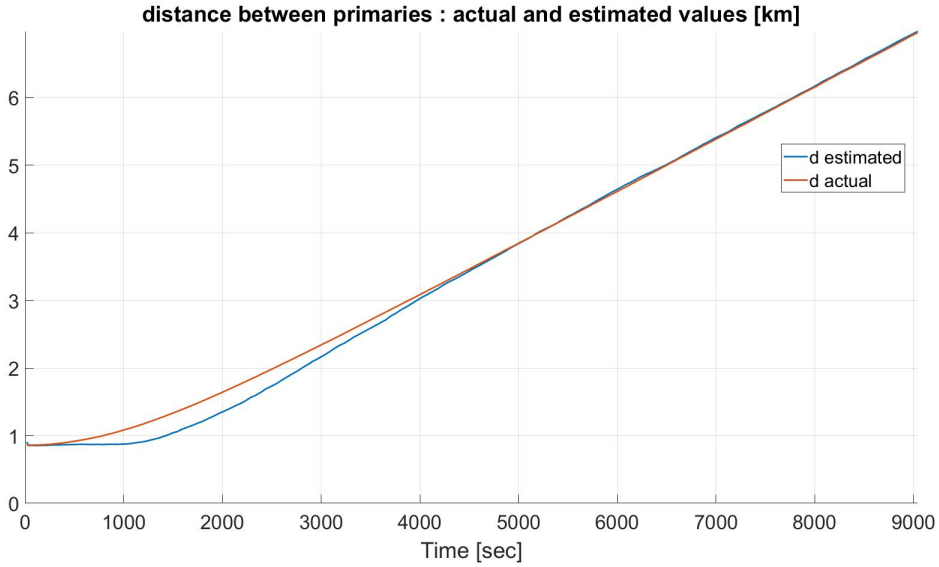

Fig. 27 Actual and estimated values of d

The initial splitting velocity $\dot{d}_0$ is null. The splitting is only due to a rotating velocity initially too high. So the acceleration $\ddot{d}$ is initially positive and then settles to zero, making $\dot{d}$ constant and positive, and thus d has a constant slope. If we set $\ddot{d} = 0$ in eq. (2), we find the equilibrium rotating velocity $\Omega^2 = \frac{Gm_{tot}}{d^3} = \Omega_{eq}^2$. Therefore, as soon as d settles to a constant slope, then it means that $\Omega(d) = \Omega_{eq}$

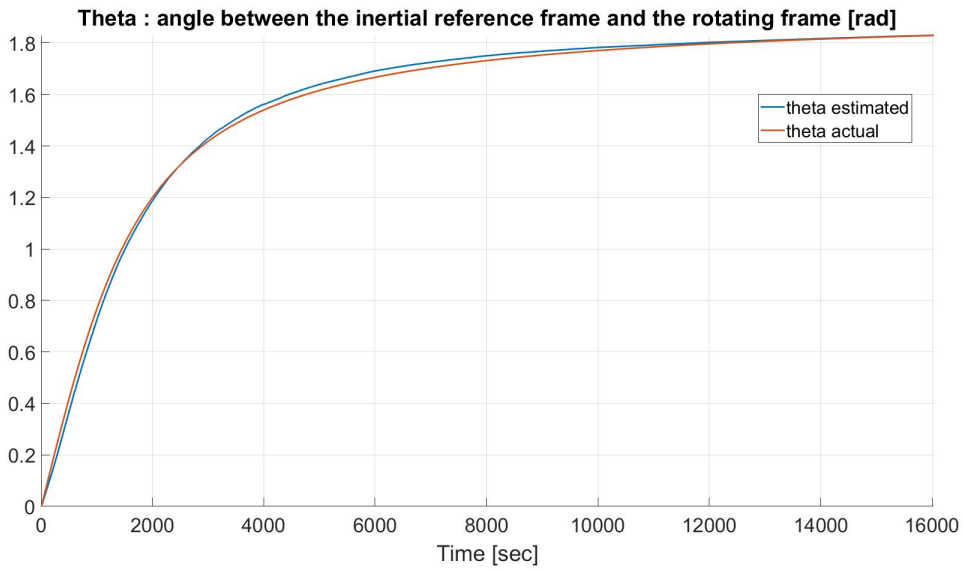

Fig. 28 Actual and estimated values of θ

As seen previously the splitting distance between primaries keep increasing because $\Omega(d) \geq \Omega_{eq}$. The rate of change of θ decreases when d increases because $\Omega(d)$ is proportional to d^{-2}. We can also see the slowing down of the rotation as a consequence of the increase of the moment of inertia of the system when the asteroids part while keeping a constant angular momentum.

Fig. 29 Actual and estimated values of μ

The convergence of the mass ratio μ is slow but still takes place. The observability condition and the EKF do not provide a time length required for the estimates to converge to their true values. Instead of increasing the length of the experiment, we can reduce the time step. Thus, for the same orbit there will be more observations, and more iterations

of the EKF, which should improve the convergence.

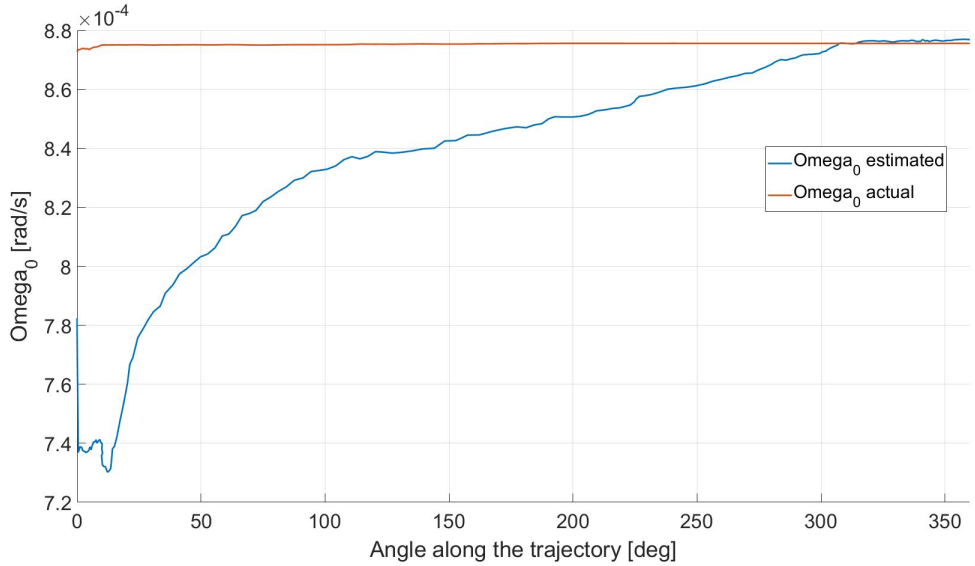

Fig. 30 Actual and estimated values of Ω_0

The estimates of Ω_0 and d_0 both improve quickly at the start and finally settle to a value closer to the actual one.

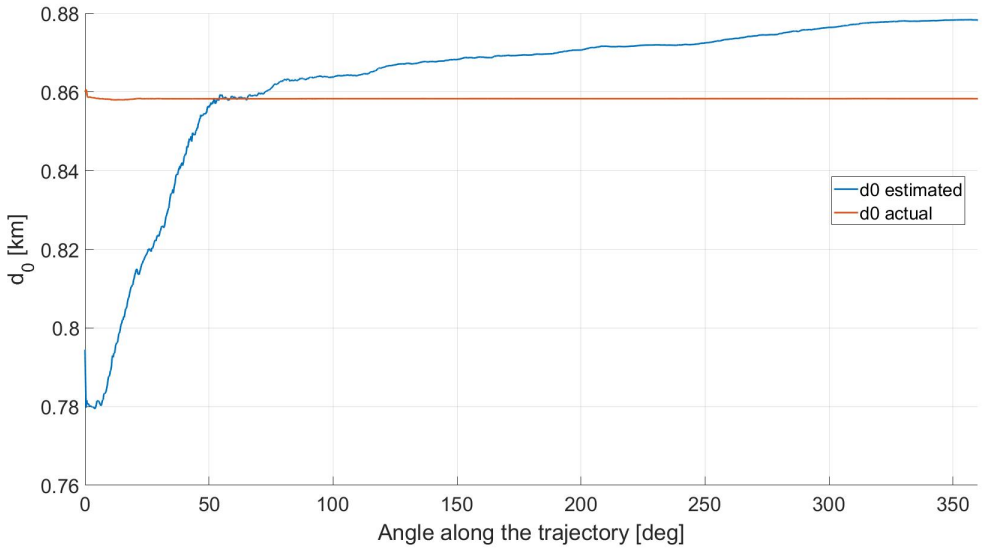

Fig. 31 Actual and estimated values of d_0

The convergence of I_n is more complicated, and should be compared with those of μ. These two parameters are related to the mass distribution of the asteroids, and are heavily affected by the spacecraft's distance to the primaries. Indeed, during part of the orbit, the spacecraft is closer to the bigger lobe, whose gravitation pull will be stronger and bias the estimates of I_n and μ. But in the end, both estimated parameters still seem to converge to a value close to the reference.

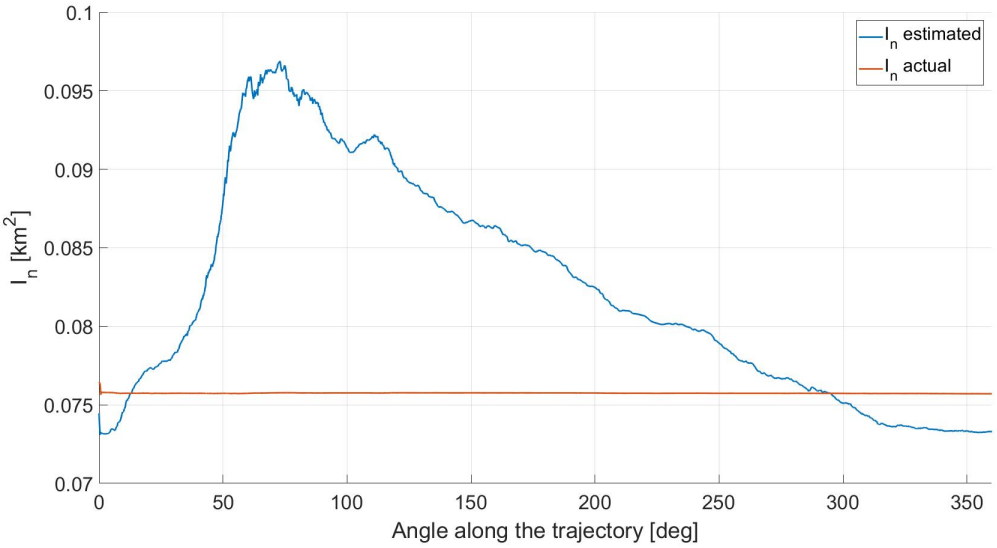

Fig. 32 Actual and estimated values of I_n

To sum up, the convergence of the estimates depends on how easily they can be inferred from the observations, but usually takes place for all parameters.

6. Conclusion

The dynamic of a splitting contact binary asteroid has been studied using the Two Body Problem frame. Several types of observation orbits around those asteroids have been compared, to finally retain elliptical orbits. A path following strategy has been implemented in an overall Indirect Adaptive Control scheme. This method can be applied to any shape of orbit, being thus more general than a Direct Adaptive Control scheme using a Trajectory Tracking algorithm. The rolling horizon parameters have been optimized to give access to the controller to a maximum of insight while keeping an efficient computation time. This process has been applied to three test cases : the asteroids Kleopatra, Castalia and 1996 HW1.

Several improvements of this method can be considered for future work, namely taking into account the mass distribution of the asteroids, to have a more detailed model of their gravitational field and thus allow proximity operations and closer orbits. A model of spheroid and ellipsoid using the Full Two and Three Body Problems described in [30] and [32] would bring a considerable accuracy improvement. The algorithm has been tested on three cases, but every time the covariance matrix Q of the EKF must be redesigned and adapted to the values of the case. An automated procedure to determine Q, would then enable to automate the whole method, whose robustness could then be tested through several Monte-Carlo simulations. The problem is also partially considered in a 3-dimensions space. Indeed, we made a restrictive assumption: the spacecraft knows that the asteroids are in a plane parallel to its inertial frame, and rotating around their shared Z-axis. This assumption can be easily relieved in a future work, and should not have a great impact on the results.

7. Bibliography

[1] Rita K. Mann, D. J. . P. L., "Fraction of Contact Binary Trojan Asteroids," *The Astronomical Journal*, 2007.

[2] JB Bouvier, K. H., and Hirabayashi, M., "Orbit Control of a Spacecraft around a Contact Binary Asteroid undergoing shape deformation," , 2019. Not submitted yet.

[3] Fujiwara, A., Kawaguchi, J., Yeomans, D., Abe, M., Mukai, T., Okada, T., Saito, J., Yano, H., Yoshikawa, M., Scheeres, D., Barnouin-Jha, O., Cheng, A., Demura, H., Gaskell, R., Ikeda, H., Kominato, T., Miyamoto, H., Nakamura, A., Nakamura, R., Sasaki, S., and Uesugi, K., "The rubble-pile asteroid Itokawa as observed by Hayabusa," *Science*, Vol. 312, 2006, pp. 1330–1334.

[4] Watanabe, S., Tsuda, Y., Yoshikawa, M., Tanaka, S., Saiki, T., and Nakazawa, S., "Hayabusa2 Mission Overview," *Space Science Reviews*, Vol. 208, 2018, pp. 3 – 16. doi:10.1007/s11214-017-0377-1.

[5] Lauretta, D., Bartels, A., Barucci, M., Bierhaus, E., Binzel, R., Bottke, W., Campins, H., Chesley, S., Clark, B., Clark, B., Cloutis, E., Connolly, H., Crombie, M., Delb, M., Dworkin, J., Emery, J., Glavin, D., Hamilton, V., Hergenrother, C., Johnson, C., Keller, L., Michel, P., Nolan, M., Sandford, S., Scheeres, D., Simon, A., B.Sutter, Vokrouhlick, D., and Walsh, K., "The OSIREX-REx target asteorid (101955) Bennu: Constraints on its physical, geological, and dynamical nature from astronomical observations," *Meteoritics & Planetary Science*, Vol. 50, 2014, pp. 834 – 849. doi:10.1111/maps.12353.

[6] Lauretta, D. S., Balram-Knutson, S. S., Beshore, E., Boynton, W. V., Drouet d'Aubigny, C., DellaGiustina, D. N., Enos, H. L., Golish, D. R., Hergenrother, C. W., Howell, E. S., Bennett, C. A., Morton, E. T., Nolan, M. C., Rizk, B., Roper, H. L., Bartels, A. E., Bos, B. J., Dworkin, J. P., Highsmith, D. E., Lorenz, D. A., Lim, L. F., Mink, R., Moreau, M. C., Nuth, J. A., Reuter, D. C., Simon, A. A., Bierhaus, E. B., Bryan, B. H., Ballouz, R., Barnouin, O. S., Binzel, R. P., Bottke, W. F., Hamilton, V. E., Walsh, K. J., Chesley, S. R., Christensen, P. R., Clark, B. E., Connolly, H. C., Crombie, M. K., Daly, M. G., Emery, J. P., McCoy, T. J., McMahon, J. W., Scheeres, D. J., Messenger, S., Nakamura-Messenger, K., Righter, K., and Sandford, S. A., "OSIRIS-REx: Sample Return from Asteroid (101955) Bennu," *Space Science Reviews*, Vol. 212, 2017, pp. 925–984. doi:10.1007/s11214-017-0405-1.

[7] Glavin, D., and Squyres, S., "An Overview of the Comet Astrobiology Exploration Sample Return (CAESAR) New Frontiers Mission," *EGU General Assembly Conference Abstracts*, EGU General Assembly Conference Abstracts, Vol. 20, 2018, p. 4823.

[8] Mazanek, D., Raymond, M., John, B., and Robert, M., "Asteroid Redirect Mission concept: A bold approach for utilizing space resources," *Acta Astronautica*, Vol. 117, 2015, pp. 163–171. doi:10.1016/j.actaastro.2015.06.018.

[9] Anderson, R. C., Scheres, D., Chesley, S., and team, B., "Binary Asteroid In-Situ Explorer Mission (BASiX): A Mission Concept to Explore a Binary Near Earth Asteroid System," *45th Lunar and Planetary Science Conference, held at The Woodlands, Texas. LPI Contribution*, Vol. 1777, 2014, p. 1571.

[10] Elvis, M., "Let's mine asteroids–for science and profit: the commercial dream of trawling space for valuable minerals could bring enormous benefits to a wide range of sciences," *Nature*, Vol. 485, No. 7400, 2012, p. 549.

[11] Cheng, A., Rivkin, A., Michel, P., Atchison, J., Barnouin, O., Benner, L., Chabot, N., Earnst, C., Fahnestock, E., Kueppers, M., Pravec, P., Rainey, E., Richardson, D., Stickle, A., and Thomas, C., "AIDA DART asteroid deflection test: Planetary defense and science objectives," *Planetary and Space Science*, Vol. 157, 2018, pp. 104 – 115. doi:10.1016/j.pss.2018.02.015.

[12] A. Harris, E. F., and Pravec, P., "On the shapes and spins of rubble pile asteroids," *Icarus*, Vol. 199, 2009, pp. 310–318. doi:10.1016/j.icarus.2008.09.012.

[13] Rozitis, B., MacLennan, E., and Emery, J. P., "Cohesive forces prevent the rotational breakup of rubble-pile asteroid (29075) 1950 DA," *Nature*, Vol. 512, No. 7513, 2014, pp. 174–176.

[14] Hirabayashi, M., and Scheeres, D., "Stress and failure analysis of rapidly rotating asteroid (29075) 1950 DA," *The Astrophysical Journal Letters*, Vol. 798, 2014, p. L8.

[15] M. Hirabayashi, H. Y. J. K. J. B., M. Morimoto, "Linear stability of collinear equilibrium points around an asteroid as a two-connected-mass: Application to fast rotating Asteroid 2000 EB 14," *Icarus*, Vol. 206, 2010, pp. 780 – 782.

[16] Richardson, D., Barnouin, O., Benner, L., Bottke, W., Bagatin, A. C., Cheng, A., Eggl, S., Hamilton, D., Hestroffer, D., Hirabayashi, M., Maurel, C., McMahon, J., Michel, P., Murdoch, N., Naidu, S., Pravec, P., Rivkin, A., Rosenblatt, P., Sarid, G., Scheeres, D., Scheirich, P., Tsiganis, K., Zhang, Y., the AIDA Dynamical, and of Didymos Working Group, P. P., "Dynamical and Physical Properties of 65803 Didymos, the Proposed AIDA Mission Target," *AAS/Division for Planetary Sciences Meeting Abstracts 48*, AAS/Division for Planetary Sciences Meeting Abstracts, Vol. 48, 2016, p. 123.17.

[17] Margot, J., Nolan, M., Benner, L., Ostro, S., Jurgens, R., Giorgini, J., Slade, M., and Campbell, D., "Binary Asteroids in the Near-Earth Object Population," *Science*, Vol. 296, 2002, pp. 1445 – 1448. doi:10.1126/science.1072094.

[18] Christopher Magri, M. C. N. b. P. A. T. b. Y. R. F. M. M. R. J. V. J. L. A. B. J. D. G. S. J. O. D. J. S. M. D. H. H. R. J. M. S. N. M. G. V. V. K. Y. N. K. I. E. M. M. W. B. J.-L. M. V. B. V. P.-B. A. G. D. H. P. K. D. P. P., Ellen S. Howell, "Radar and photometric observations and shape modeling of contact binary near-Earth Asteroid (8567) 1996 HW1," *Icarus*, Vol. 214, 2011, pp. 210 – 227.

[19] Hudson, R. S., and Ostro, S. J., "Shape of Asteroid 4769 Castalia (1989 PB) from Inversion of Radar Images," *Science*, Vol. 263, 1994, pp. 940 – 943.

[20] Eric DeJong, D. S., Scott Hudson, and Suzuki, S., "Asteroid 4179 Toutatis," Tech. rep., JPL, 2003. URL `https://echo.jpl.nasa.gov/asteroids/4179_Toutatis/toutatis.html`.

[21] Michael K. Shepard, D. S. L. B. J. D. G. E. S. H. C. M. M. C. N. A. S. P. A. T. A. V., Bradley Timerson, "A revised shape model of asteroid (216) Kleopatra," *Icarus*, Vol. 311, 2018, pp. 197 – 209.

[22] Levy, S., "The Extended Kalman Filter: An Interactive Tutorial for Non-Experts," , ???? [retrieved 20 September 2018] at $https://home.wlu.edu/levys/kalman_tutorial/$.

[23] Schneider, R., and Georgakis, C., "How to NOT Make the Extended Kalman Filter Fail," *Industrial and Engineering Chemistry Research*, 2013, pp. 3354–3362.

[24] Timm Faulwasser, P. Z., Tobias Weber, and Findeisen, R., "Implementation of Nonlinear Model Predictive Path-Following Control for an Industrial Robot," *IEEE Transactions on Control Systems Technology*, Vol. 25, 2017, pp. 1505 – 1511.

[25] Lavretsky, E., "Adaptive Control: Introduction, Overview, and Applications," , ????

[26] Howard Kaufman, I. B., and Sobel, K., *Direct Adaptive Control Algorithms, Theory and Applications*, 2nd ed., Springer, 1998.

[27] Astolfi, A., and Ortega, R., "Immersion and Invariance: A New Tool for Stabilization and Adaptive Control of Nonlinear Systems," *IEEE Transactions on Automatic Control*, Vol. 48, 2003. doi:10.1109/TAC.2003.809820.

[28] Werner, R., and Scheeres, D., "Exterior Gravitation of a Polyhedron derived and compared with Harmonic and Mascon Gravitation Representations of Asteroid 4769 Castalia," *Celestial Mechanics and Dynamical Astronomy*, 1996.

[29] Scheeres, D., "Orbital Mechanics about Small Bodies," *Acta Astronautica*, Vol. 72, 2012, pp. 1 – 14. doi:10.1016/j.actaastro.2011.10.021.

[30] Bellerose, J., and Scheeres, D., "Energy and Stability in the Full Two Body Problem," *Celestial Mechanics and Dynamical Astronomy*, 2008. doi:10.1007/s10569-007-9108-3.

[31] Scheeres, D., "Rotational fission of contact binary asteroids," *Icarus*, 2007. doi:10.1016/j.icarus.2007.02.015.

[32] Bellerose, J., and Scheeres, D., "General Dynamics in the Restricted Full Three Body Problem," *Acta Astronautica*, 2008. doi:10.1016/j.actaastro.2008.01.018.

[33] Tsuchiyama, A., Uesugi, M., Matsushima, T., Michikami, T., Kadono, T., Nakamura, T., Uesugi, K., Nakano, T., Sandford, S., Noguchi, R., Matsumoto, T., Matsuno, J., Nagano, T., Imai, Y., Takeuchi, A., Suzuki, Y., Ogami, T., Katagiri, J., Ebihara, M., Ireland, T., Kitajima, F., Nagao, K., Naraoka, H., Noguchi, T., Okazaki, R., Yurimoto, H., Zolensky, M., Mukai, T., Abe, M., Yada, T., Fujimura, A., Yoshikawa, M., and Kawaguchi, J., "Three-Dimensional Structure of Hayabusa Samples: Origin and Evolution of Itokawa Regolith," *Science*, Vol. 333, 2011, pp. 1125 – 1128. doi:10.1126/science.1207807.

[34] K. Walsh, D. R., and Michel, P., "Rotational breakup as the origin of small binary asteroids," *Nature*, Vol. 454, 2008. doi:10.1038/nature07078.

[35] Kumpati S. Narendra, L. S. V., "Direct and Indirect Model Reference Adaptive Control," *7th IFAC World Congress on A Link Between Science and Applications of Automatic Control*, Vol. 15, edited by Automatica, International Federation of Automatic Control, 1978, pp. 653 – 664.

[36] Boyd, S., and Sastry, S., "Necessary and Sufficient Conditions for Parameter Convergence in Adaptive Control," *Automatica*, Vol. 22, 1986, pp. 629–639.

[37] Chowdhary, G., and Johnson, E., "Concurrent Learning for Convergence in Adaptive Control without Persistency of Excitation," *49th IEEE Conference on Decision and Control*, 2010, pp. 3674–3679.

[38] J. Junkins, M. A., and Robinett, R., "Nonlinear Adaptive Control of Spacecraft Maneuvers," *Journal of Guidance, Control and Dynamics*, Vol. 20, 1997. doi:10.2514/2.4192.

[39] S. Bandyopadhyay, S. C., and Hadaegh, F., "Nonlinear Attitude Control of Spacecraft with a Large Captured Object," *Journal of Guidance, Control and Dynamics*, Vol. 39, 2016. doi:10.2514/1.G001341.

[40] P. Singla, K. S., and Junkins, J., "Adaptive Output Feedback Control for Spacecraft Rendezvous and Docking Under Measurement Uncertainty," *Journal of Guidance, Control and Dynamics*, Vol. 29, 2006. doi:10.2514/1.17498.

[41] Seo, D., and Akella, M., "High-Performance Spacecraft Adaptive Attitude-Tracking Control Through Attracting-Manifold Design," *Journal of Guidance, Control, and Dynamics*, Vol. 31, 2008. doi:10.2514/1.33308.

[42] John E Prussing, B. A. C., *Orbital Mechanics*, Oxford University Press, USA, 1993.

[43] D. J. Scheeres, R. S. H., S. J. Ostro, and Werner, R. A., "Orbits Close to Asteroid 4769 Castalia," *Icarus*, Vol. 121, 1996, pp. 67 – 87.

[44] Koon, W. S., Lo, M. W., Marsden, J. E., and Ross, S. D., "Dynamical Systems, the Three-Body Problem and Space Mission Design," , April 2011.

[45] Szebehely, V., *Theory Of Orbits : the Restricted Problem Of Three Bodies*, Academic Press, 1967.

[46] Song, Y., and Grizzle, J., "The Extended Kalman Filter as a Local Asymptotic Observer for Nonlinear Discrete-Time Systems," *1992 American Control Conference*, 1992, pp. 3365–3369. doi:10.23919/ACC.1992.4792775.

[47] Eberly, D., "Distance from a Point to an Ellipse, an Ellipsoid, or a Hyperellipsoid," , 2013.

[48] Xiao-Diao Chen, G. W. J.-C. P. G. X., Jun-Hai Yong, "Computing the minimum distance between a point and a NURBS curve," *Elsevier, Computer-Aided Design*, Vol. 40, 2008, pp. 1051 – 1054.

[49] Luca, A. D., "Trajectory Tracking Control," , ????

[50] B. Alagoz, C. Y., A. Ates, and Senol, B., "An experimental investigation for error-cube PID control," *Transactions of the Institute of Measurement and Control*, Vol. 37, 2015, p. 652 – 660. doi:10.1177/0142331214527476.

[51] Bindu B Jagannatha, J.-B. B., and Ho, K., "Preliminary Design of Low-Energy Low-Thrust Transfers to Halo Orbits using Feedback Control," *The American Institute of Aeronautics and Astronautics Journal*, 2018.

[52] Valappil, J., and Georgakis, C., "Systematic Estimation of State Noise Statistics for Extended Kalman Filters," *American Institute of Chemical Engineers Journal*, Vol. 46, 2000.

Appendix A. Details of the Jacobian F

$$
\mathbf{F} = \frac{\partial \mathbf{f}}{\partial \mathbf{X}} =
\left[\begin{array}{cccc|cccc|c|cccc}
0 & 0 & 0 & 0 & 1 & 0 & 0 & 0 & 0 & 0 & 0 & 0 & 0 \\
0 & 0 & 0 & 0 & 0 & 1 & 0 & 0 & 0 & 0 & 0 & 0 & 0 \\
0 & 0 & 0 & 0 & 0 & 0 & 1 & 0 & 0 & 0 & 0 & 0 & 0 \\
0 & 0 & 0 & 0 & 0 & 0 & 0 & 1 & 0 & 0 & 0 & 0 & 0 \\
\hline
\frac{\partial f_5}{\partial x} & \frac{\partial f_5}{\partial y} & \frac{\partial f_5}{\partial z} & \frac{\partial f_5}{\partial d} & 0 & 2\Omega & 0 & \frac{\partial f_5}{\partial \dot{d}} & 0 & \frac{\partial f_5}{\partial \mu} & \frac{\partial f_5}{\partial \Omega_0} & \frac{\partial f_5}{\partial d_0} & \frac{\partial f_5}{\partial I_n} \\
\frac{\partial f_6}{\partial x} & \frac{\partial f_6}{\partial y} & \frac{\partial f_6}{\partial z} & \frac{\partial f_6}{\partial d} & -2\Omega & 0 & 0 & \frac{\partial f_6}{\partial \dot{d}} & 0 & \frac{\partial f_6}{\partial \mu} & \frac{\partial f_6}{\partial \Omega_0} & \frac{\partial f_6}{\partial d_0} & \frac{\partial f_6}{\partial I_n} \\
\frac{\partial f_7}{\partial x} & \frac{\partial f_7}{\partial y} & \frac{\partial f_7}{\partial z} & \frac{\partial f_7}{\partial d} & 0 & 0 & 0 & 0 & 0 & \frac{\partial f_7}{\partial \mu} & 0 & 0 & 0 \\
0 & 0 & 0 & \frac{\partial f_8}{\partial d} & 0 & 0 & 0 & 0 & 0 & \frac{\partial f_8}{\partial \mu} & \frac{\partial f_8}{\partial \Omega_0} & \frac{\partial f_8}{\partial d_0} & \frac{\partial f_8}{\partial I_n} \\
\hline
0 & 0 & 0 & -\frac{2\mu(1-\mu)d\Omega}{I_n+\mu(1-\mu)d^2} & 0 & 0 & 0 & 0 & 0 & \frac{\partial \Omega}{\partial \mu} & \frac{\partial \Omega}{\partial \Omega_0} & \frac{\partial \Omega}{\partial d_0} & \frac{\partial \Omega}{\partial I_n} \\
\hline
0 & 0 & 0 & 0 & 0 & 0 & 0 & 0 & 0 & 0 & 0 & 0 & 0 \\
0 & 0 & 0 & 0 & 0 & 0 & 0 & 0 & 0 & 0 & 0 & 0 & 0 \\
0 & 0 & 0 & 0 & 0 & 0 & 0 & 0 & 0 & 0 & 0 & 0 & 0 \\
0 & 0 & 0 & 0 & 0 & 0 & 0 & 0 & 0 & 0 & 0 & 0 & 0
\end{array}\right]
$$

Details of the Jacobian H

$$
\mathbf{H} = \frac{\partial \mathbf{h}}{\partial \mathbf{X}} = \left[\begin{array}{cccc|cccc|ccccc}
cos(\theta) & -sin(\theta) & 0 & \mu cos(\theta) & 0 & 0 & 0 & 0 & \frac{\partial h_1}{\partial \theta} & \frac{\partial h_1}{\partial \mu} & \frac{\partial h_1}{\partial \Omega_0} & \frac{\partial h_1}{\partial d_0} & \frac{\partial h_1}{\partial I_n} \\
sin(\theta) & cos(\theta) & 0 & \mu sin(\theta) & 0 & 0 & 0 & 0 & \frac{\partial h_2}{\partial \theta} & \frac{\partial h_2}{\partial \mu} & \frac{\partial h_2}{\partial \Omega_0} & \frac{\partial h_2}{\partial d_0} & \frac{\partial h_2}{\partial I_n} \\
0 & 0 & 1 & 0 & 0 & 0 & 0 & 0 & 0 & 0 & 0 & 0 & 0 \\
-\Omega sin(\theta) & -\Omega cos(\theta) & 0 & \frac{\partial h_4}{\partial d} & cos(\theta) & -sin(\theta) & 0 & \mu cos(\theta) & \frac{\partial h_4}{\partial \theta} & \frac{\partial h_4}{\partial \mu} & \frac{\partial h_4}{\partial \Omega_0} & \frac{\partial h_4}{\partial d_0} & \frac{\partial h_4}{\partial I_n} \\
\Omega cos(\theta) & -\Omega sin(\theta) & 0 & \frac{\partial h_5}{\partial d} & sin(\theta) & cos(\theta) & 0 & \mu sin(\theta) & \frac{\partial h_5}{\partial \theta} & \frac{\partial h_5}{\partial \mu} & \frac{\partial h_5}{\partial \Omega_0} & \frac{\partial h_5}{\partial d_0} & \frac{\partial h_5}{\partial I_n} \\
0 & 0 & 0 & 0 & 0 & 0 & 1 & 0 & 0 & 0 & 0 & 0 & 0 \\
\hline
cos(\theta) & -sin(\theta) & 0 & -(1-\mu)cos(\theta) & 0 & 0 & 0 & 0 & \frac{\partial h_7}{\partial \theta} & \frac{\partial h_7}{\partial \mu} & \frac{\partial h_7}{\partial \Omega_0} & \frac{\partial h_7}{\partial d_0} & \frac{\partial h_7}{\partial I_n} \\
sin(\theta) & cos(\theta) & 0 & -(1-\mu)sin(\theta) & 0 & 0 & 0 & 0 & \frac{\partial h_8}{\partial \theta} & \frac{\partial h_8}{\partial \mu} & \frac{\partial h_8}{\partial \Omega_0} & \frac{\partial h_8}{\partial d_0} & \frac{\partial h_8}{\partial I_n} \\
0 & 0 & 1 & 0 & 0 & 0 & 0 & 0 & 0 & 0 & 0 & 0 & 0 \\
-\Omega sin(\theta) & -\Omega cos(\theta) & 0 & \frac{\partial h_{10}}{\partial d} & cos(\theta) & -sin(\theta) & 0 & -(1-\mu)cos(\theta) & \frac{\partial h_{10}}{\partial \theta} & \frac{\partial h_{10}}{\partial \mu} & \frac{\partial h_{10}}{\partial \Omega_0} & \frac{\partial h_{10}}{\partial d_0} & \frac{\partial h_{10}}{\partial I_n} \\
\Omega cos(\theta) & -\Omega sin(\theta) & 0 & \frac{\partial h_{11}}{\partial d} & sin(\theta) & cos(\theta) & 0 & -(1-\mu)sin(\theta) & \frac{\partial h_{11}}{\partial \theta} & \frac{\partial h_{11}}{\partial \mu} & \frac{\partial h_{11}}{\partial \Omega_0} & \frac{\partial h_{11}}{\partial d_0} & \frac{\partial h_{11}}{\partial I_n} \\
0 & 0 & 0 & 0 & 0 & 0 & 1 & 0 & 0 & 0 & 0 & 0 & 0
\end{array}\right]
$$